Alma Mater Studiorum – Università di Bologna

SCUOLA DI SCIENZE

Dipartimento di Chimica Industriale "Toso Montanari"

Corso di Laurea Magistrale in

Chimica Industriale

Classe LM – 71 –Scienze e Tecnologie della Chimica Industriale

A synthetic route for atropisomeric atorvastatin

Tesi di laurea sperimentale

CANDIDATO

Michele Para

RELATORE

Prof. Andrea Mazzanti

CORRELATORE

Dr. Michele Mancinelli

Sessione III

Anno Accademico 2017-2018

Abstract

The aim of the thesis is to insert a chiral axis on the atorvastatin molecule without having a quaternary carbon, but by blocking the rotation of the single Carbon-Carbon bond of the aryl in position 3, to obtain stable atropisomers.

This type of molecules can interact with the HMGR enzyme differently depending on the atropisomer taken into consideration, increasing or lowering the inhibition constant of the drug.

Docking calculations were made, starting from the interaction of the atorvastatin with the HMGR, comparing them with the calculations of atorvastatin differently substituted in the aryl in position 3, obtaining a library of possible products.

The chiral axis was introduced in the position 3 of the pyrrole ring, because it does not affect the active sites of the atorvastatin, but could give new interactions with the enzyme, depending on the substituent.

At the same time, we tried to obtain an efficient synthesis path for having different substituted aryl in the 3 position, increasing the steric hindrance to obtain stable atropisomers. DFT calculations were made to optimize the geometries of the ground and transition states of the test molecules, to forecast the activation energy to rotation.

The synthetized products were characterized by NMR (^{1}H, ^{13}C, DEPT), and by analysing the experimental rotational energy barriers with different techniques such as variable temperature NMR (VT-NMR), Dynamic HPLC (DHPLC) and kinetic studies.

The absolute configuration of stable atropisomers was assigned with the simulation of the ECD spectra.

Riassunto

Lo scopo della tesi è di inserire un asse chirale nella molecola di atorvastatina bloccando la rotazione del legame Carbonio-Carbonio dell'arile in posizione 3, ottenendo atropisomeri stabili.

Questo tipo di molecole così ottenute possono interagire con l'enzima HMGR in modo diverso a seconda dell'atropisomero preso in considerazione, aumentando o diminuendo la costante di inibizione del farmaco.

Sono stati fatti calcoli di docking molecolare partendo dall'interazione dell'atorvastatina con l'HMGR e confrontandoli con i calcoli di atorvastatina diversamente sostituita in posizione 3, ottenendo una libreria di possibili prodotti.

Per ottenere l’asse chirale è stata scelta la posizione 3 dell'anello pirrolico poiché esso non influenza direttamente i siti attivi dell'atorvastatina, ma potrebbe dare nuove interazioni a seconda del sostituente scelto.

Nello stesso tempo abbiamo ottimizzato il percorso sintetico per immettere arili stericamente ingombranti in posizione 3 dell’anello pirrolico, ottenendo atropisomeri stabili. Inoltre, sono stati effettuati calcoli DFT per ottimizzare le geometrie degli stati fondamentali e di transizione delle molecole target.

Infine abbiamo caratterizzato i prodotti sintetizzati mediante NMR (^{1}H, ^{13}C, DEPT 1.5) e analizzato le barriere energetiche rotazionali con tecniche diverse quali NMR a temperatura variabile (VT-NMR), HPLC dinamico (DHPLC) e studi cinetici.

La configurazione assoluta degli atropisomeri stabili è stata effettuata con il metodo ECD.

Index

1. Introduction

Statins are a class of drugs biologically active in the inhibition of the enzyme 3-hydroxy-3-methyl-glutaryl-coenzyme A reductase (HMGR).

Liver enzyme HMGR catalyses the formation of mevalonate, the key step in the biosynthesis of intracellular cholesterol[1] and terpenoids (a kind of steroids). In particular, cholesterol is a type of lipid molecule, it is biosynthesized by all animals cells because is an essential structural component of cellular membrane and is a precursor for the biosynthesis of steroid hormones, bile acid and vitamin D.

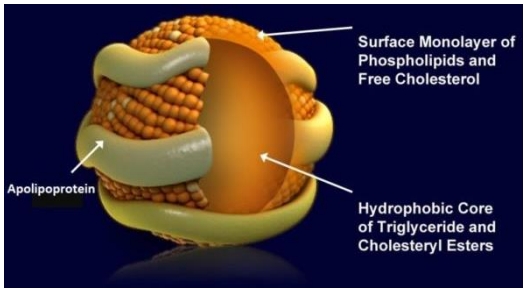

Figure 1: Lipoprotein structure [Feingold K-R, Grunfeld C. - Introduction to Lipids and Lipoproteins]

Cholesterol is insoluble in water, and to reach the cells it must be transported in association with proteins. Lipoproteins are complex particles with a hydrophobic central core containing cholesterol esters (or triglycerides) surrounded by an hydrophilic membrane consisting of free cholesterol, phospholipids and apolipoproteins, Thanks this form the cholesterol can be driven in the blood's plasma [Figure 1]. Plasma lipoproteins are divided into seven classes based on size, lipid composition and apolipoproteins associated, are individuated like: *chylomicrons, chylomicron remnants, very low density lipoproteins (VLDL), intermediate density lipoproteins (IDL), low density lipoprotein (LDL), high density lipoproteins (HDL) and lipoprotein (a) (Lp (a))*.[2] A correct balance of this mixture of compounds is essential for the correct supply of cholesterol in the human body, whereas an high concentration of LDL, for example, could cause coronary heart diseases, stroke or even death.

1.1. Development of the studies

The first study on this lipid began in the 1910 when Windaus reported that atherosclerotic plaques from aortas of humans subject contains over 20-fold higher concentrations of cholesterol than normal aortas did. The research were largely rejected, or not followed, until the 1940s, due to a prevailing view that the diseases were simple consequences of aging and it could not be prevented.

During the '50s, John Gofman, after epidemiologic study of the cholesterol-coronary connection, correlated the heart attacks with elevated levels of blood cholesterol, but also that the cholesterol was contained in LDL, using the newly developed ultracentrifuge to separate plasma lipoproteins by flotation. He also observed that heart attacks were less frequent when the blood contained elevated level of HDL.[3]

In the following ten years the connection between blood cholesterol and coronary atherosclerosis was firmly established, showing that the risk was increased by a number of other factors such as high blood pressure and smoking. These conclusions increased the interest to determine the biological pathway of cholesterol synthesis in the body.

This pathway involves more than 30 enzymatic reaction and was discovered only in the 1960 by four biochemists: Konrad E. Bloch, Feodor Lynen, John Cornforth, and George Popják. They determined the synthesis in four stages: 1) condensation of three acetate units to form a six-carbon intermediate, mevalonate; 2) conversion of mevalonate to activated isoprene units; 3) polymerization of six isoprene units to form carbon linear squalene; 4) cyclization of squalene to form the steroid nucleus, with a further series of changes to produce cholesterol.[4] [Figure 2]

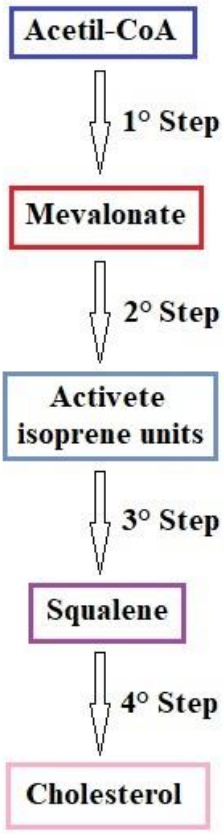

Figure 2: byosinthesis simplified of cholesterol

Therefore, by inhibiting one of these 4 steps, it is possible to control cholesterol synthesis and avoid related pathologies.

In 1964 thanks to these studies, Konrad E. Bloch and Feodor Lynen ware awarded of the Nobel prize in "Physiology or

Medicine", for their discoveries concerning "*the mechanism and regulation of the cholesterol and fatty acid metabolism"*.[5]

In the first '70s the biologist Akira Endo developed the first active pharmaceutical ingredient (API) with the classification of statins: compactin. Starting with animals and humans tests, in the 1976 the project expired soon due to some dosage problem in the experiment with dogs and monkey (they received 100-200 mg/Kg per day when the human tests were at max 25 mg/Kg per day, but compactine was efficient with just 1 mg/Kg per day).[3]

The interest in the cholesterol metabolism did not decrease and in 1985 Michael S. Brown and Joseph L. Goldstein won the Nobel Prize for "revolutionized our knowledge about *the regulation of cholesterol metabolism and the treatment of diseases caused by abnormally elevated cholesterol levels in the blood"*. They found out that on the cells surface there are receptors which mediate the uptake of LDL. That research showed the importance of the cholesterol in the blood but pointed out that the excess of LDL accumulates in the walls of arteries forming bulky plaques that choke the blood flow until a clot eventually forms, obstructing the artery and causing a heart attack or stroke.[6] The first commercial statin was lovastatin, developed by Merck and approved by U.S. Food and Drug Administration (FDA) in 1987 [Figure 3]. Since that year, several API were developed that concur with the HMG-CoA to block the synthesis of the cholesterol.

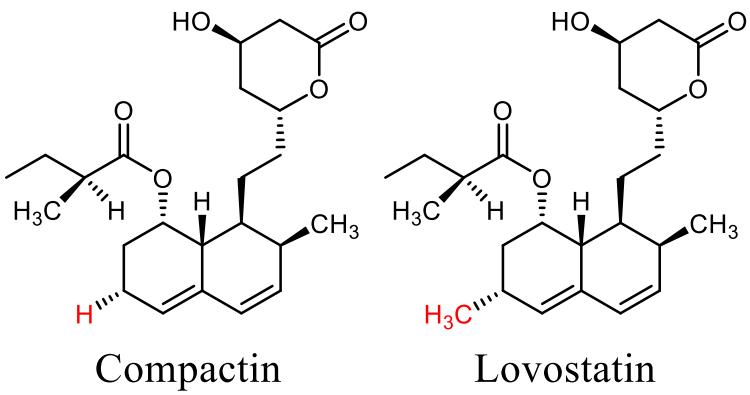

Figure 3: Structures of compactin and lovostatin.

Today the most selling statins are Lipitor and Crestor which contain the optimized APIs, atorvastatin and rosuvastatin [Figure 4]. Using data from the 2005 to 2008 the "U.S. Centers for Disease Control and Prevention" estimate that 25% of adults over age 45 used those powerful statins and between 1999 and 2007 the death associated with heart disease decreased by 28%.

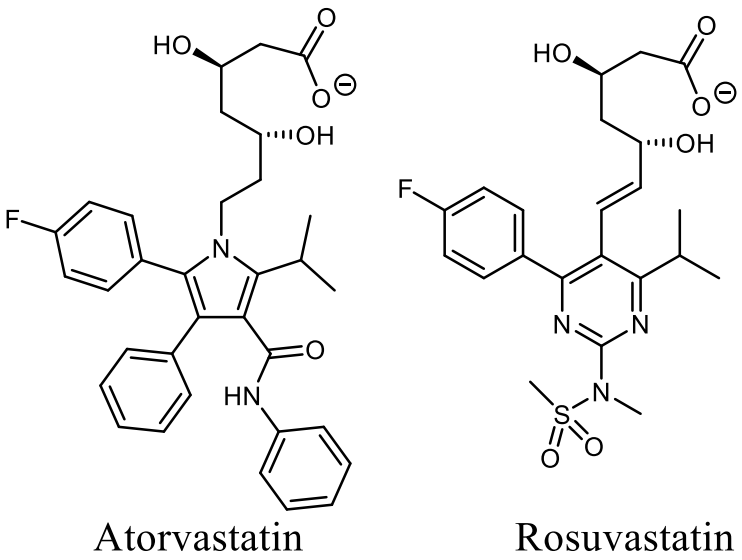

Figure 4: structure of atorvastatin(Lipitor) and rosuvastatin (Crestor)

In 2010 Pfizer gained more than $ 5.3 milliard selling Lipitor (atorvastatin).[7]

1.2. HMG-CoA Reductase and atorvastatin

The HMGR is an enzyme that can be found in eukaryotes (class I, bound in the endoplasmic reticulum) and prokaryotes (class II, soluble on cytoplasm). The proteins are organized in dimers, each one contains two active sites formed by residue from both monomers. The complete structure forms a tetramer.[Figure 5] [8]

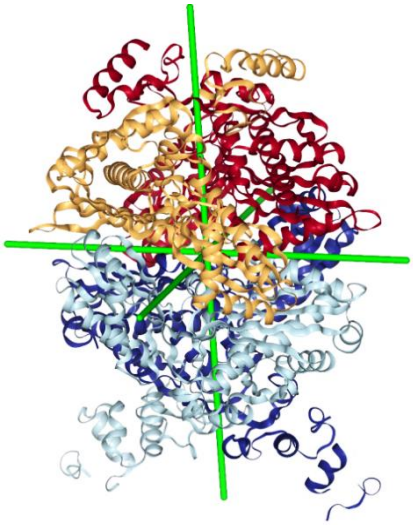

Figure 5: 3D conformation of HMGR, each colour represent a monomer of protein, the red and the yellow ones formed a dimer like the grey and blue ones. In green are evidenced the 2D symmetry [Protein Data Bank – protein n° 1HWK]

The enzyme present in the human liver is a class I solved by High-Resolution Crystallization, the proteins analysed show four domains: catalytic, linker, anchor and the polypeptide residue. The anchor allows to bind the reticulum and the linker connect the anchor to the core region that is the catalytic domain. This portion of proteins is composed by three principal domains, the N-Domain, the L-Domain, and the S-Domain. The L-domain is unique to HMGRs while the S-domain, forms the binding site for NADP. [Figure 6].

The S and L domains are connected by a *cis-loop* which is essential for the HMG-binding site.

The active site of HMG-CoA reductase is at the interface of the homodimer, between a monomer that binds the NADPH and a second monomer that binds the HMG-CoA. [9]

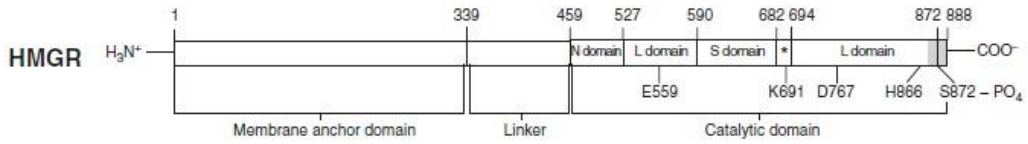

Figure 6: structure of the protein *Human HMGR*

The statins are developed to bind with the HMG portion of HMG-CoA binding pocket (characterized by the *cis-loop*) with their polar part, and then the non-polar region occupies a portion of the coenzyme.

The binding of HMG-CoA with the enzyme HMGR, in the biosynthesis of cholesterol, is the rate-limiting step. According to Konrad E. Bloch and Feodor Lynen, the formation of mevalonate is the first step for the synthesis. [Figure 7]

This step is a four-electron reductive deacylation of HMG-CoA to CoA and mevalonate using 2 molecules of NADPH and 2 H^+.

(*S*)-HMG-CoA + 2 NADPH + 2 H^+ → (*R*)-mevalonate + 2 $NADP^+$ + CoA-SH

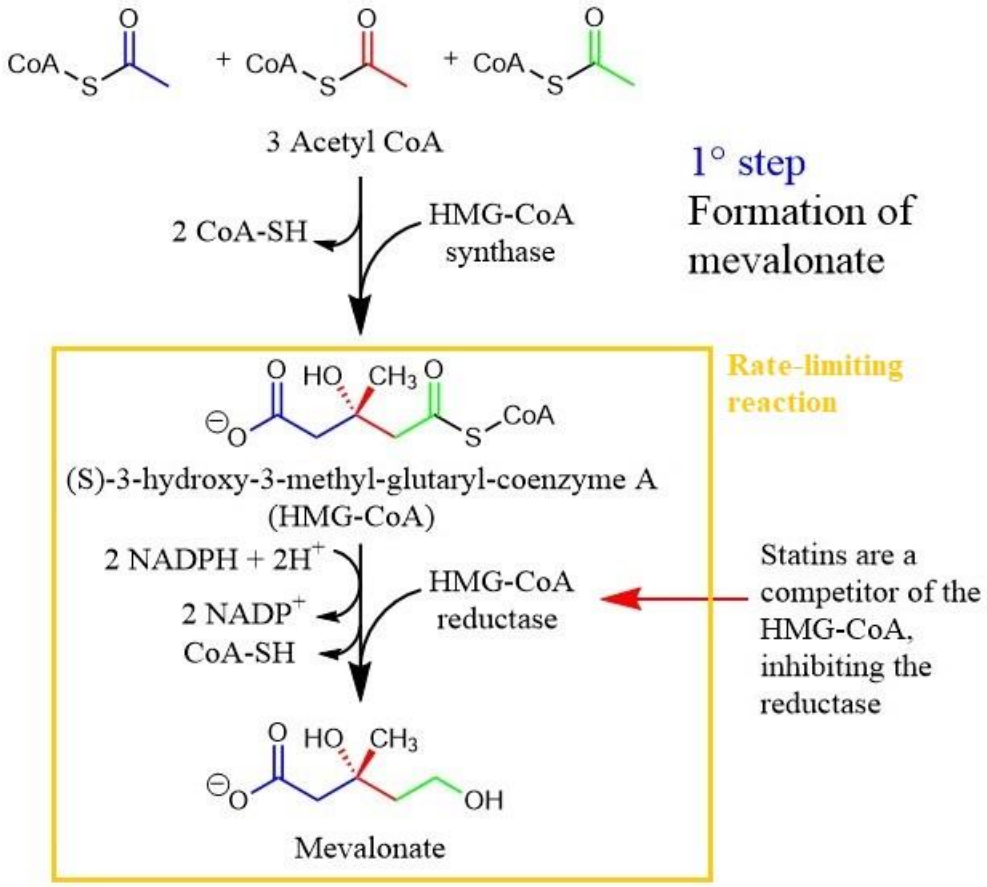

Figure 7: Biosynthesis of cholesterol st step, the rate-limiting reaction is the formation of (*R*)-mevalonate

The statins are sold in an inactive lactone form or like salt. In vivo the lactone form is enzymatically hydrolysed to its active hydroxyl-acid form and is covalently linked to the hydrophobic groups. The chiral chain is the focus point of the inhibitors, because the drugs need to replace the biologic reagent to inhibit the biosynthesis.

Statins are classified in two group: type 1, like lovastatin, pravastatin and simvastatin, are molecules that derives from reassembling of the substituted decaling-ring structure of compactin [Figure 3]; type 2, like atorvastatin, fluvastatin, cerivastatin and rosuvastatin, [Figure 4, Figure] are fully synthetic inhibitors that generally show a minor inhibition constant than the other type. We pointed our attention on the atorvastatin for the further studies.

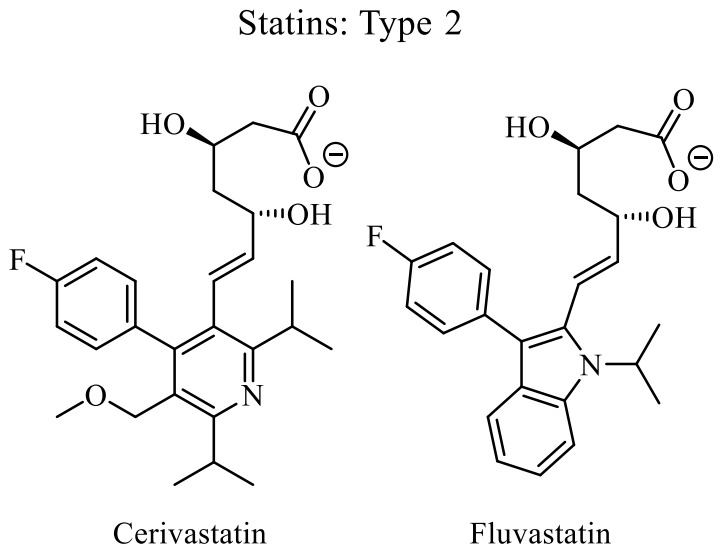

Figure 8: Synthetic Statins

Atorvastatin, sold as calcium salt under the trade name Lipitor® by Pfizer, was approved for medical use in the United States in 1996. Now it is available as a generic medication.

It has been partially designed basing on molecular modelling of structure of the fungal metabolites, the compactine. The goal of the studies was to perform a drug with a lower inhibition constant (K_i), that reflects the binding affinity of the drug with the enzyme. It is expressed in molarity, and represent the dissociation constant of the enzyme-inhibitor complex. Thus its numeric value represents the amount of medication needed to inhibit the enzyme and it is used to predict clinically relevant drug interactions, and to compare the efficiency of different inhibitor. Usually the inhibition constant (K_i) is the most important indicator for drugs with the same effect.[10]

The development of atorvastatin started from the possibility that the hexaydronaphthalene portion of compactine and lovostatin could be replaced with a simpler ring system, without loss of biological activity. This disclosure supported the hypothesis that the requirement for a potent inhibitor was the 3,5-dihydroxy-heptanoic

acid or the lactone form. The easier methods of the preparation and the various possible substitution punched the development of the study for a pyrrole ring core.

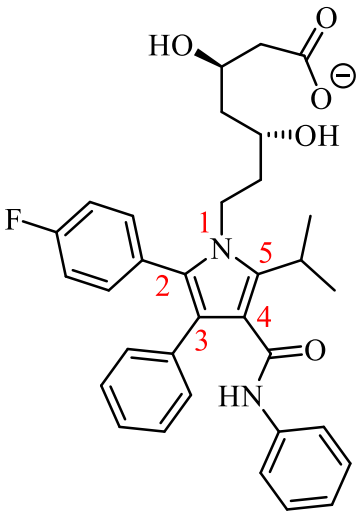

Atorvastatin

Figure 9: numeration relative at the pyrrole ring of atorvastatin

After many attempts, the position 1 of pyrrole were linked to the heptane-chain, whereas the position 5 has to be occupied by a substituent with a size not bigger than 5.9 Å, and the 2-substituent should not be not bigger than 3.3 Å. The groups that demonstrated the lowest inhibition constant were the 4-fluorophenyl in position 2 and the isopropyl in position 5, but this compound showed one-tenth of the inhibitory potency of compactine. These tests demonstrated that the 3 and 4 position need to be occupied to have an optimal inhibition. The chlorines and bromine were shelved for incoming toxicity and the best activity was found with a phenyl group in position 3, and a carboxiamidophenyl group in position 4. [Figure 9]

Both *in-vivo* and *in-vitro* experiments demonstrated that (+)-atorvastatin [(3*R*,5*R*)-7-(2-(4-fluorophenyl)-5-isopropyl-3-phenyl-4-(phenylcarbamoyl)-1H-pyrrol-1-yl)-3,5-dihydroxyheptanoic acid] was actually more potent and efficacious than lovastatin in lowering LDL cholesterol in rabbits and guinea pigs, and triglycerides in rats, with useless afford for the opposite enantiomer. The choice to develop the pure stereoisomer was done both for ethical and market reasons.[11]

The estimate reduction of the risk is: for acute coronary heart disease 36%, rate of stroke by 48%, the coronary revascularisation is gain to 31%. Atorvastatin reduces the death rate of patient at risk by 28%.[12] Although the benefits are numerous, any drug has different side effects that can hamper the desire to continue the treatment. For the atorvastatin there are serious side effect that involves muscles breakdown, kidney damages or liver problems (they are considerable *rare* because involves about 0.1% of the patient) or less serious side effects like nausea, headaches or nosebleeds (they are considerable *common* because involves about 1% of the patient).[13] Considering that the statins are prescribed more and more frequently, the improvement of their efficiency is an ambitious target for lowering the active dosage and to reduce side-effects.

1.3. Chirality and Atropisomerism

When a given molecule and its mirror image are not superimposable, the object is defined like *chiral*. To make this situation possible the molecule must lack a symmetry plane or an inversion centre. The phenomenon of the chirality is usually linked at the tetrahedral structure of carbon, when connected with 4 different substituents. The two mirror images not superimposable are defined enantiomers. The enantiomers are two identical molecules, which have the same physical proprieties like melting point, boiling point, density and solubility.

They have the same amount of relative energy but the chemistry in a chiral ambient is different, for example when they react with another chiral reagent, like in enzymatic reactions. The different reaction mechanism is due to the different spatial conformation of the enantiomers that can expose or hide a particular reaction site.

This is true for the HMG-CoA or the heptane-chain in atorvastatin because the relative mirror images are different and only one form can proceed in the synthesis of the cholesterol. [Figure 10].

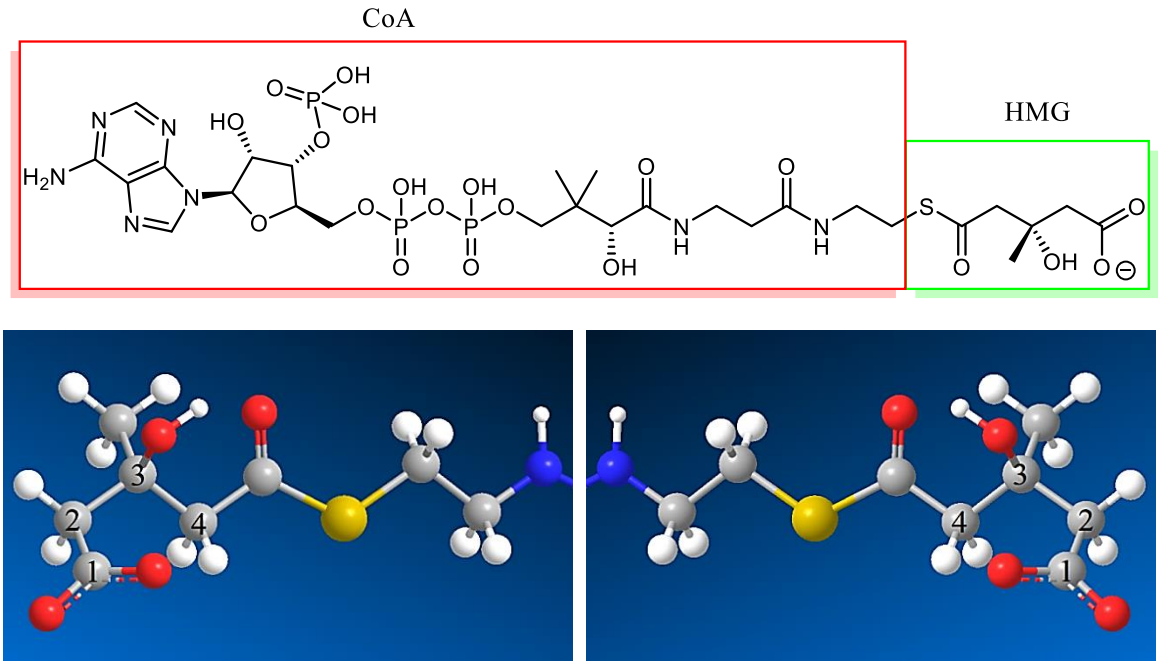

Figure 10: Complete structure of the (*S*)-HMG-CoA and mirror images of the chiral structure that interact with the catalytic portion of the enzyme.

In the case of atropisomers the chirality is due to the restricted rotation around a single bond for the steric hindrance and/or electronics factor. The most famous example is the (2,2′-bis(diphenylphosphino)-1,1′-binaphthyl) known as BINAP [Figure 11].[14]

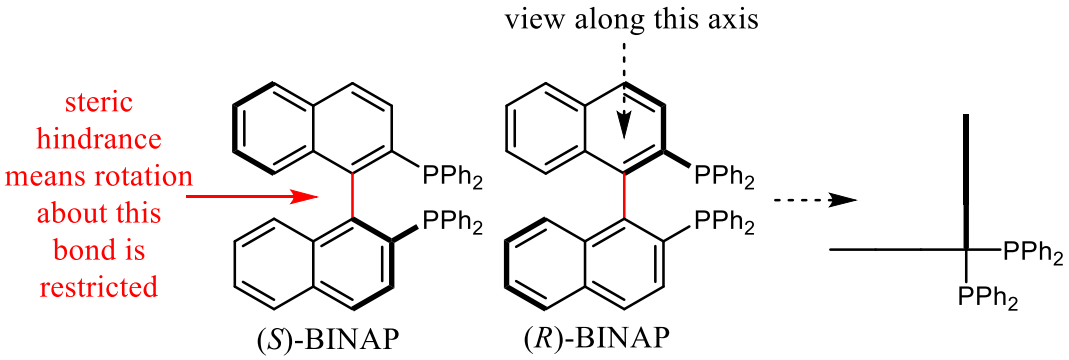

Figure 11: spatial disposition of BINAP [taken from Jonathan Clayden, Nick Greeves and Stuart Warren - Organic Chemistry]

Atropisomers are involved in a chemical equilibrium that is thermally dependent, they differ in this way from many other types of chiral structure because the interconversion from each other occurs without breaking and reforming of covalent bonds. In 1983 Oki proposed a boundary rule to define atropisomers from conformers, with his arbitrary definition that atropisomers are conformers which interconvert with a half-life ($t_{1/2}$) of at least 1000 s at +25 °C, corresponding to a rotational energy barriers (ΔE_{rot}) of 21.8 kcal/mol.[15] With this barrier the physical separation is possible but this notion is not exhaustive. LaPlante proposed later an energy scale of stereogenic axis stability, dividing the atropisomers into three classes, based on the values of rotational energy [Figure 12].

The first class are compounds that have fast axial rotation rates on the order of seconds or faster, exhibit no axial chirality and $\Delta E_{rot} \leq 20$ kcal/mol. This is the simplest and most common class of compound, they are developed as purified, single compounds and no extraordinary analytical strategies need to be implemented.

The second class are compounds that have a metastable situation in which the rotational barriers are between 20 and 30 kcal/mol, with a $t_{1/2}$ that spans from few minutes to weeks. Molecules with these features are expected to show some observable indication of the presence of atropisomers. However the less stable of these components cannot always be physically resolved at +25 °C. This class is therefore divided in to two subclasses:

2a) 20 kcal/mol $\leq \Delta E_{rot} \leq$ 23 kcal/mol. The two enantiomers can be clearly detected and sometimes resolved, but the racemisation process is fast enough to maintain a pure

enantiomer for only several second (at +25 °C). The complete racemisation occurs in less than 1 hour, these process are so fast that the compounds can be considered like single entity.

2b) 23 kcal/mol ≤ ΔE_{rot} ≤ 30 kcal/mol. In this sub-class the enantiomers can be detected, resolved and stored as single enantiomerically pure atropisomer at +25 °C for hours or even weeks.

Class three: compounds with ΔE_{rot} ≥ 30 kcal/mol show very slow torsion-rotation rates with $t_{1/2}$ on the order of years. These chiral compounds are stable over time and thus can be isolated as optically pure, stored as part of a pharmaceutically relevant formulation for a period of time consistent with the required shelf life, and dosed as a single compound. Development can proceed in a similar manner as "classical" stereoisomers that result from classic chiral centers. If the calculated rotational barrier of a compound is high, is possible to envisage the developing of atropisomeric compound as a single, pure, stereochemically stable isomer. [16]

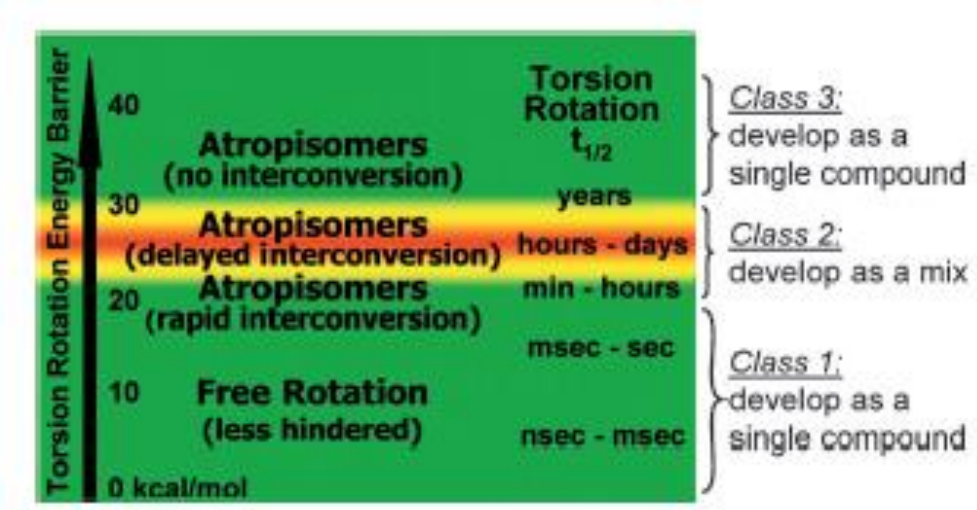

Figure 12: Qualitative guide developed by LaPlant, O. Hucke et. al to help correlate the calculated rotational barrier, $t_{1/2}$ and compound classes for predicting development strategy. [Steven R. LaPlante,* Paul J. Edwards, Lee D. Fader, Araz Jakalian, and Oliver Hucke - Revealing Atropisomer Axial Chirality in Drug Discovery]

Given the absence of a stereogenic centre, the absolute configuration of axially chiral conformers is assigned using the concept of helicity based on a dihedral angle that involves the rotation. The dihedral angle is defined by four atoms **a-b-c-d** and represents

the torsion angle between two planes **a-b-c** (yellow one) and **b-c-d** (blue one), from -180° to +180° [Figure 13].

In the assignment of absolute configuration of chiral axis, the bond between **b** and **c** forms the chiral axis while **a** and **d** are the substituent of highest priority (selected with the CIP rules) on each side of the bond.

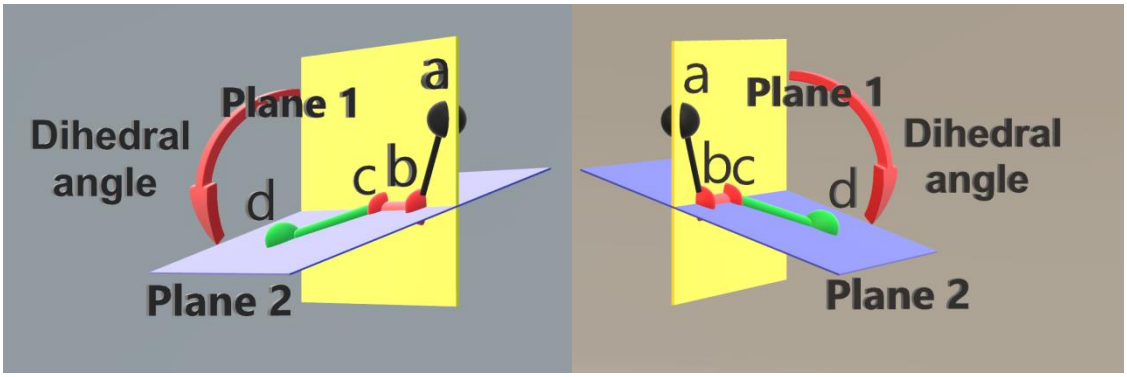

Figure 13: Schematic definition of configuration of a chiral axis: the first immage rappresent an *M* configuration and the second a *P* configuration.

Looking from the closest atom (**a**) and moving along the shortest path to the substituent of highest priority on the other side (**d**), the absolute configuration is assigned *P* (Plus, from 0° to + 180°) in clockwise and *M* (Minus, from 0° to -180°) in counter clockwise.

During our studies we can prove the differences between the two atropisomers computing the inhibition constant of the single enantiomers with the protein, noting that one chiral axis can fits in a efficiently way than the other.

1.4. Docking Calculations

Our studies aims to obtain a chiral axis on the pyrrole scaffold without having a quaternary stereogenic carbon, by changing the aryl ring in position 3 with the aim to obtain stable atropisomers. This new stereogenic element can interact with the enzyme in different ways, with the goal to lowering the inhibition constant of the drug.

The first modelling of the molecules was driven by initial docking calculation. We used the AutoDock4 free program that can predict the bound conformation and binding energies of ligand and the macromolecular targets. The results are expressed in binding free energy (ΔG°), defined by the free energy of the complex (ligand bound to the enzyme) minus the free energies of the ligand and the enzyme separately in aqueous solution.[17]

To explore the large conformational space available to a ligand around a protein, the program uses a grid-based method for a rapid evaluation of the binding energy of trial conformation. In this method the movement of the ligand are restricted in a grid, then the molecule is sequentially placed at each grid point. The conformational searching is a Lamarckian genetic algorithm that create populations of trial conformation, than using a semiempirical free energy force field, the program predicts the binding free energies of small molecule to macromolecular targets, the interaction energy between the ligand and the target is computed and stored.

The trial conformation mutate, exchange conformational parameters, searching individuals with lowest binding energy. The “Lamarckian” aspect is to search the local conformational space, finding local minima of the ligand and then pass this information to later generations but treating the enzyme like completely rigid. The force field is based on comprehensive thermodynamic model that allows incorporation of intramolecular energies into the predicted free energy of binding, performed by evaluating energies for both the bound and unbound states.

The results of the simulations are incorporated in a graph that shows the distribution of the conformation with the relative binding free energy. This makes possible to find the geometries that have the lowest ΔG° (with a standard error about 2-3 kcal/mol) and then expand for the value of predicted inhibition constant and ligand efficiency. [18]

The computation of the binding energy of different molecules has enabled us to define a library of different substituent that have large steric hindrance in position 3 of the pyrrole core of atorvastatine, without interactions with the key substituent of the enzyme. However, the calculation of the energy required to the racemisation of a single atropisomers needs higher level calculations, such as density functional theory (DFT).

In order to make easier the synthesis and the calculation we decided to continue the study on a simpler model of atorvastatin molecule, without the chiral heptane-chain and without the parafluorophenyl ring.

2. Aim of the studies

The aim of this thesis is the design a preparation of new cores of atorvastatines, with axial chirality due to a stereogenic axis in position 3 of the pyrrole core, looking for stable atropisomers. [Figure 14]

The second target is to provide a new efficient synthetical strategy which will allow in the future to be completed by adding the missing parts of true atorvastatine.

The compounds taking into account have a *o*-tolyl, 1-naphthalene and 2,3-dimethyl-naphthalene group in position 3 of pyrrole. Several synthetic routes were analysed to gain the desired products, with a synthetic route that was as much as possible adaptable to different substituents, without the use of toxic or dangerous reagents.

At the end of the study were obtained, the desired final products with a low total yield but with a net increase in the added value and, a solid synthesis that can be further improved to obtain higher yields.

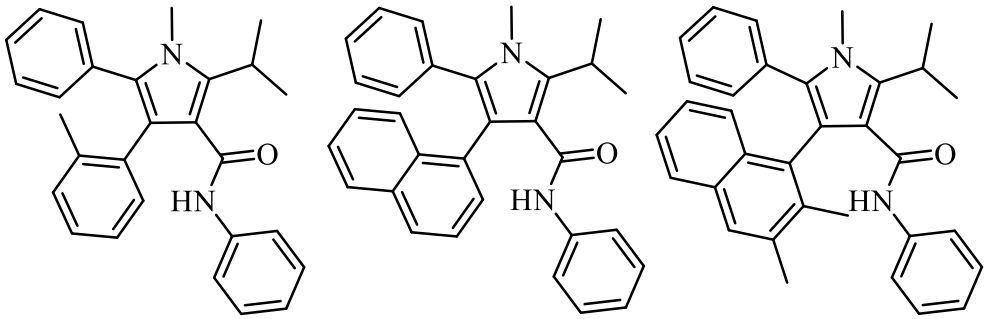

10a **10b** **10c**

Figure 14: products obtained with different synthetic ways

The rotational barriers were analysed with different spectroscopic techniques. Dynamic NMR was used for compound **10a**; compound **10b** was analysed with Dynamic HPLC. Compound **10c**, having the biggest steric hindrance, showed two atropisomers that were separable at room temperature, and they were analysed with kinetical studies and the absolute configuration are assigned with the ECD method and TD-DFT calculations.

3. Result and discussion

3.1. Conformational analysis

The studies of the energy barriers and the synthesis were focused on the atorvastatin model, with the *para*-fluorophenyl group substituted by a simpler phenyl group and t dihydroxyheptanoate-chain was replaced by a single methyl group. These simple structural changes allow us to design a more economical synthetic way, and the final products can be easily analysed with NMR spectroscopy .[Figure 15]

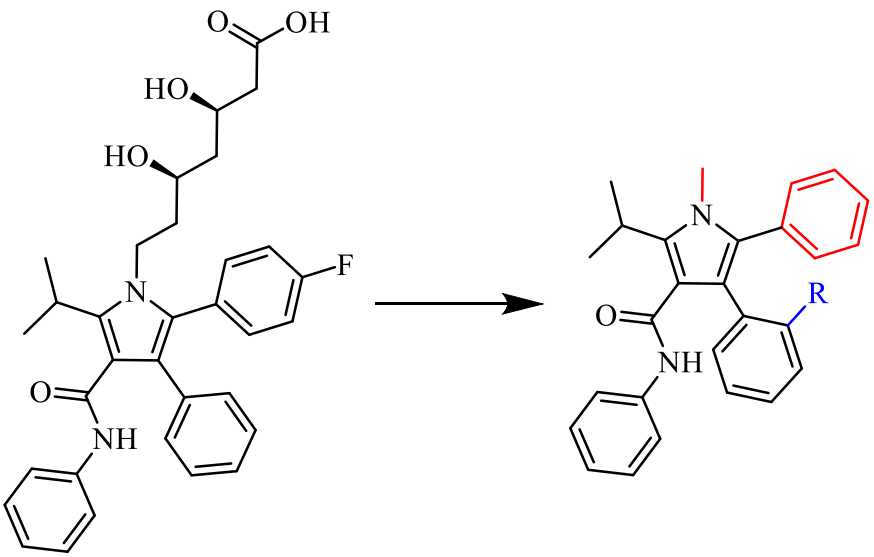

Figure 15 : Left atorvastatin, right the products prepared in this work.

The stereogenic axis in position 3 of the pyrrole can be realized by using an *ortho*-substituted aryl ring, that is forced out of the pyrrole plane, thus producing the *P* and *M* enantiomeric conformations.

A peculiarity of atorvastatin itself is that the substituent in positions 2, positions 3, and 4 of the pyrrole are twisted out the pyrrole ring. When the *ortho* substituent is added, the molecule can rearrange in a geared system: the torsional motions of two or more substituents in a molecule may be therefore strongly coupled. This situation implies that correlated rotation becomes energetically preferred over the independent rotation of the individual groups.

For every different substituent the forecast different geometry are originate by the geared position of the perpendicular group (position *a* turned clockwise and *b* turned counterclockwise) in combination with the different geometry that the *i*-propyl group can

afford (position *c* with the H point the N-metyl group and *d* with the H point the amide group). We can predict 4 GS: *ac; ad; bc; bd.* Each ground state define the relative energy amount concern to a couple of enantiomers in a total of 8 not superimposable molecules the most populate GS is that one shows the lowest relative energy at 25°C.

The different computations show that sometime even the dihedral angle of the methyl group in position 1 make possible other 2 different geometries (8 possible GS so 16 enantiomers) but are configuration barely stable and with a ΔE very low.

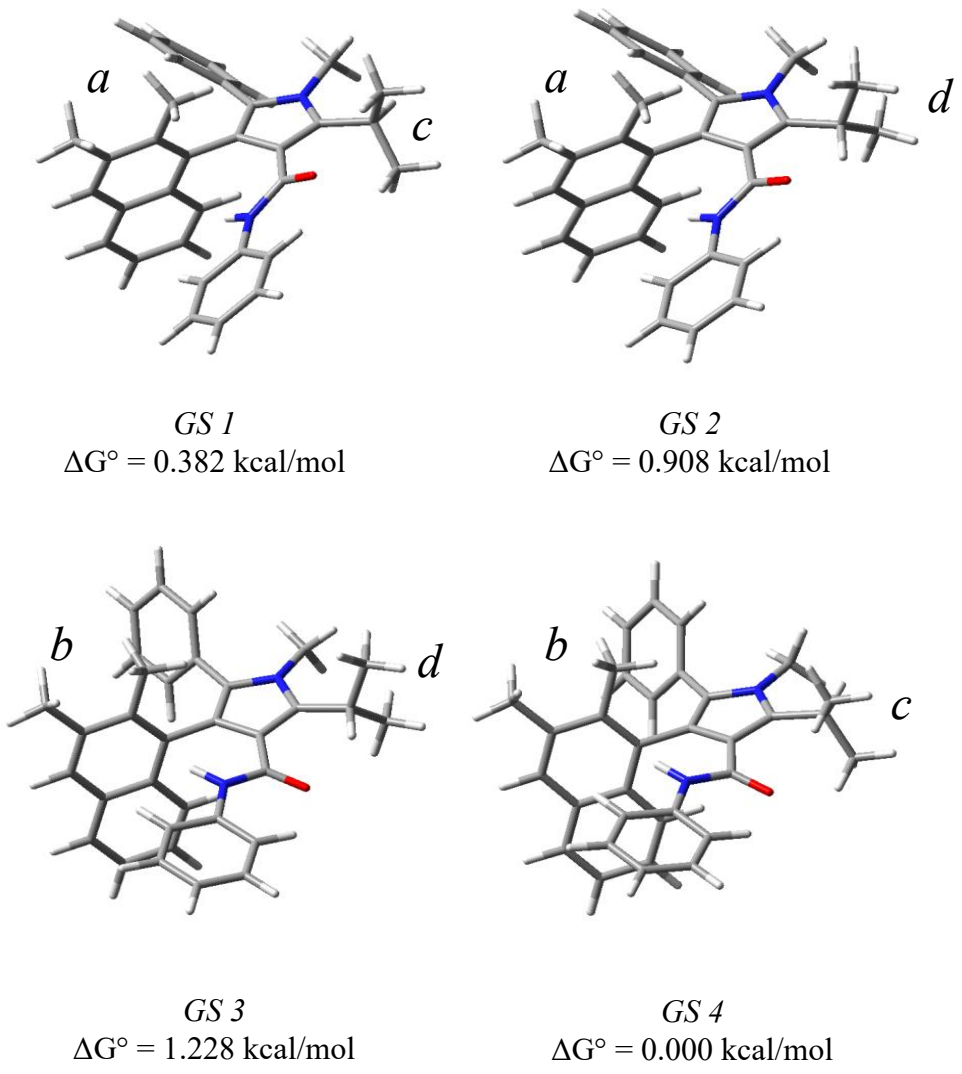

GS 1
ΔG° = 0.382 kcal/mol

GS 2
ΔG° = 0.908 kcal/mol

GS 3
ΔG° = 1.228 kcal/mol

GS 4
ΔG° = 0.000 kcal/mol

Figure 16: The letters *a, b, c,* d represent the different position that the substituents can assume. Theoretical studies performed at the B3LYP/6-31G(d) level of theory on the model system, [4-(2,3-dimethylnaphthalen-1-yl)-2-isopropyl-1-methyl-N,5-diphenyl-1H-pyrrole-3-carboxamide]. The position of the substituents determine the relative energy associate.

After a molecular mechanics scan of the potential energy surface (PES), the resulting optimized geometries were further optimized with DFT at the B3LYP/6-31G(d) level of

theory. In the case of compound **10c** four energy minima were found to be enclosed into a narrow energy range. The four conformations are different because of the disposition of the isopropyl group, and by the orientation of the amide and of the phenyl in position 2. [Figure 16]

To evaluate theΔG_{rot} of the molecule is necessary to imagine a plausible TS starting from the lowest energy GS. The expected TSs must have the *ortho* substituent coplanar with the pyrrole ring, in order to convert the chiral axis from *P* to *M*, or *vice versa*. The rotation around the chiral axis is possible from 90° to 0° (called TS-0) or from 90° to 180° (called TS-180). [Figure 17]

In the TS geometries, the molecule need to bend and deform to make the racemization possible. The racemization occurs by the lowest energy path between TS-0 and TS-180.

In the case of compound **10c** the two TSs have roughly the same energy (37.7 kcal/mol), so there is not a clear preference.

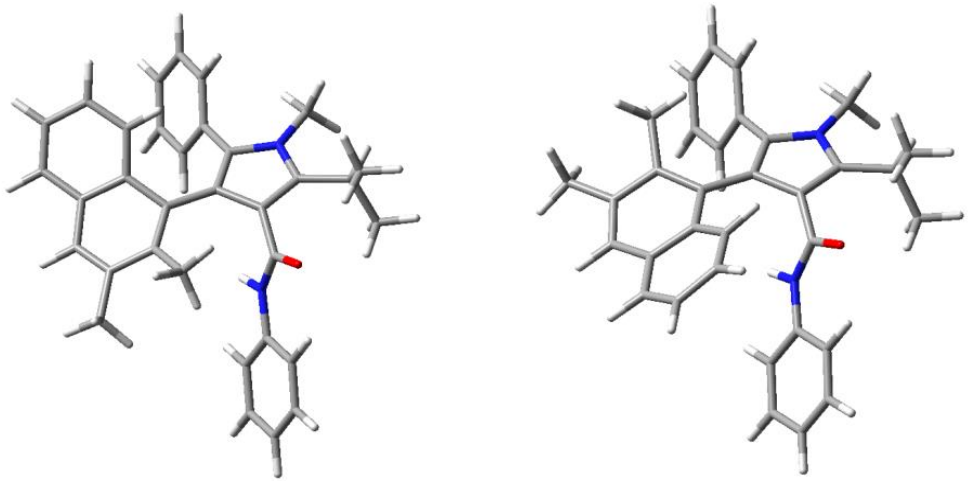

TS 0
$\Delta G^{\neq}_{calc}$ = 37.687 kcal/mol

TS 180
$\Delta G^{\neq}_{calc}$ = 37.740 kcal/mol

Figure 17: Theoretical studies performed at the B3LYP/6-31G(d) level of theory on the model system, [4-(2,3-dimethylnaphthalen-1-yl)-2-isopropyl-1-methyl-N,5-diphenyl-1H-pyrrole-3-carboxamide]. The analysis on the transition states evaluate the stability of the rotational stereoisomers.

3.1. Synthesis

As a first attempt, the preparation of the target compounds was planned as presented in Figure 18. The purpose of this pathway was to obtain the encumbered atorvastatin with a multi component reaction (MCR) [reaction *d*] with the nitro-alkene, 3-methyl-2-oxo-N-phenylbutanamide and methylamine. While the formation of the amide **3** worked smoothly with good yields, the reaction for the formation of the nitroalkene was unsuccessful, probably because of the steric hindrance of the *ortho* substituent of the benzaldehye used in the reaction.

Synthetic pathway I

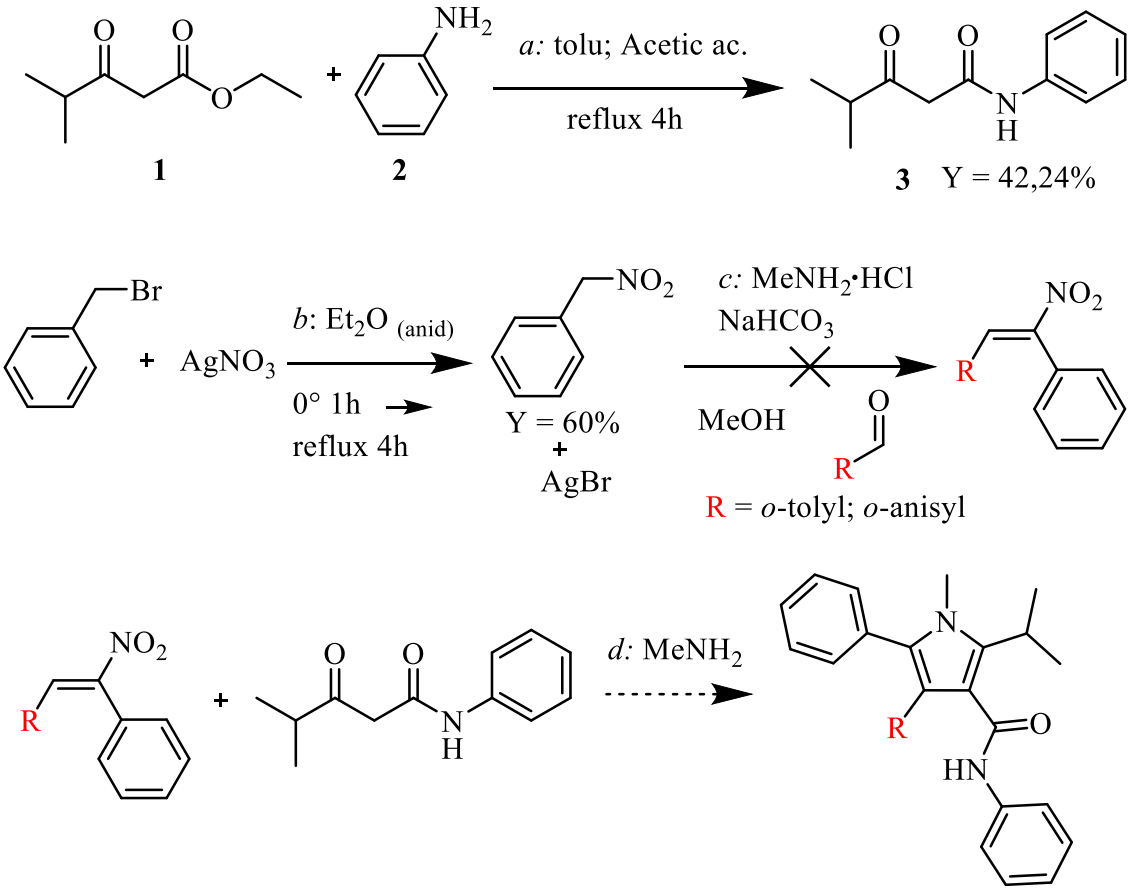

Figure 18: first synthetic way proposed

The ethyl 4-methyl-3-oxopentanoate **1** react with aniline to form compound **3** in a reaction of ammonolysis, the reaction is quite slow and rarely reaches completeness, but experimentally it is very simple without using expensive or dangerous reagents. The

compound **1** can be recovered under chromatography column, the desired product can also be purified by crystallization. [Figure 19][19]

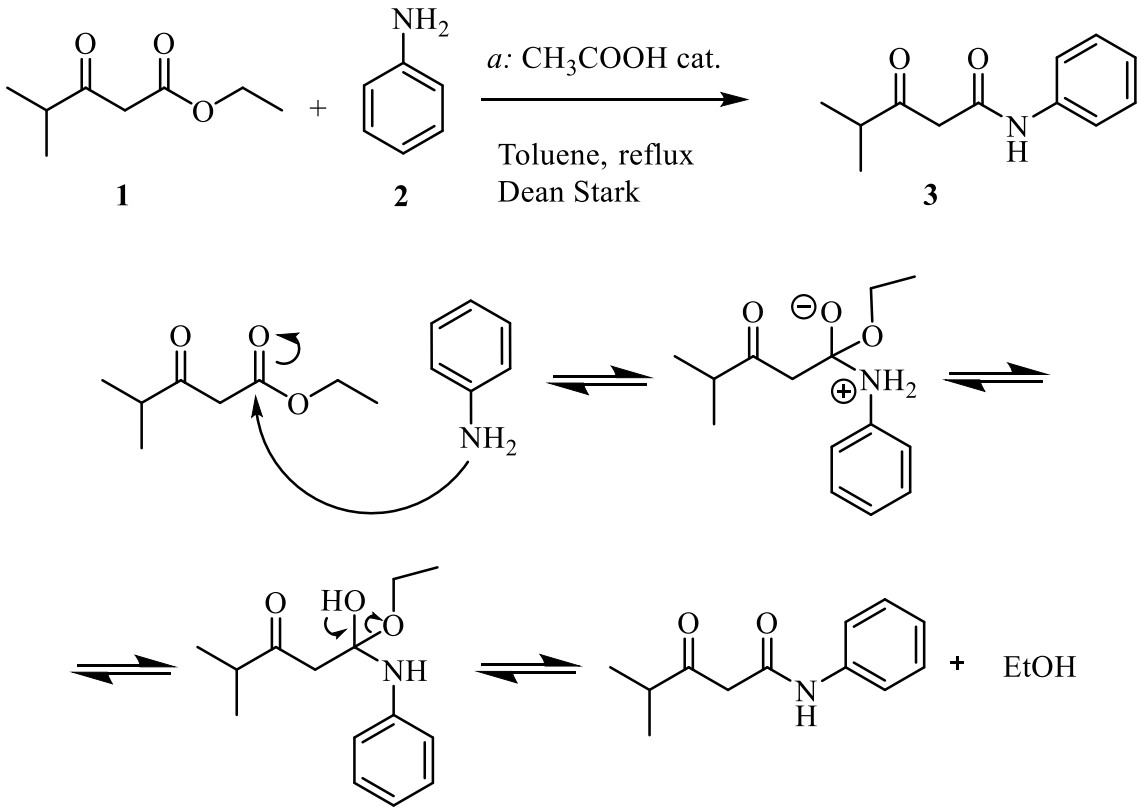

Figure 19: ammonolysis of ethyl 4-methyl-3-oxopentanoate with aniline

Product **3** remains a necessary compound for the synthesis of atorvastatin. Given that the yields obtained and reported do not exceed 65% in future studies this step can be optimized to maximize the efficiency of the reaction.

The reaction *b* with benzylbromide is an electronic substitution made by the NO_2^- ion on the bromide, driven by the formation of the AgBr salt that precipitates.[20] The second step, [reaction *c* and *e* to *p*] is the activation of the aldehyde with a primary ammine to form an imine, that can react with a Michael reaction with the phenylnitromethane to form a new C-C bond, with the consecutive dehydration to form the π bond. [Figure 20].[21-22-23-24-25-26] Several reaction conditions were tested, but all the test were unsuccessful.

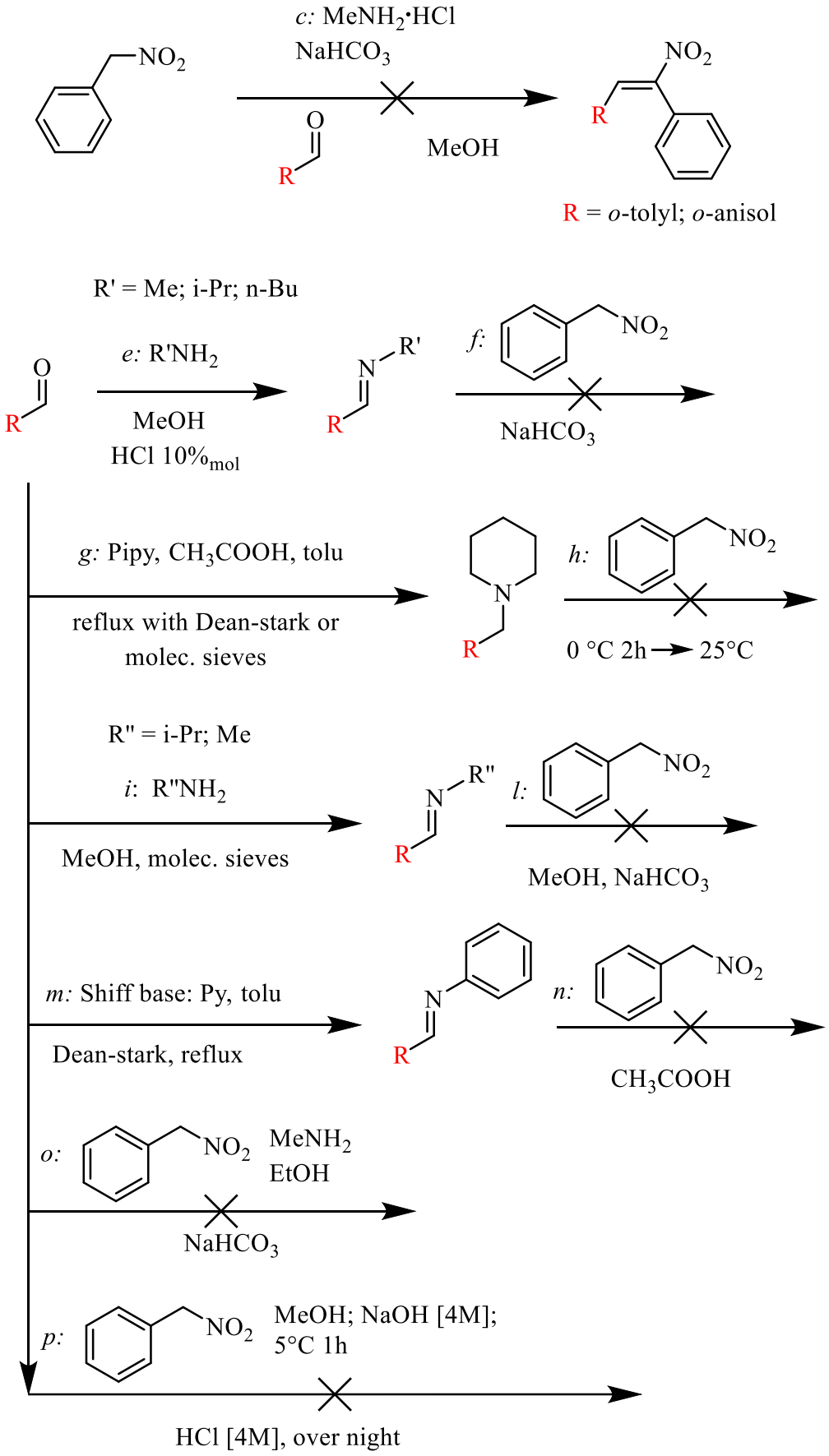

Figure 20: attempt to make possible the attack by the nitro-compound to the activated aldehyde

Since the direct attack on the nitromethylbenzene was not possible, we decided to build the alkene by a first attack from nitromethane, followed by bromination, and then using a Suzuki-Miyaura cross coupling reaction (synthetic pathway II). [Figure 21]

Synthetic pathway II

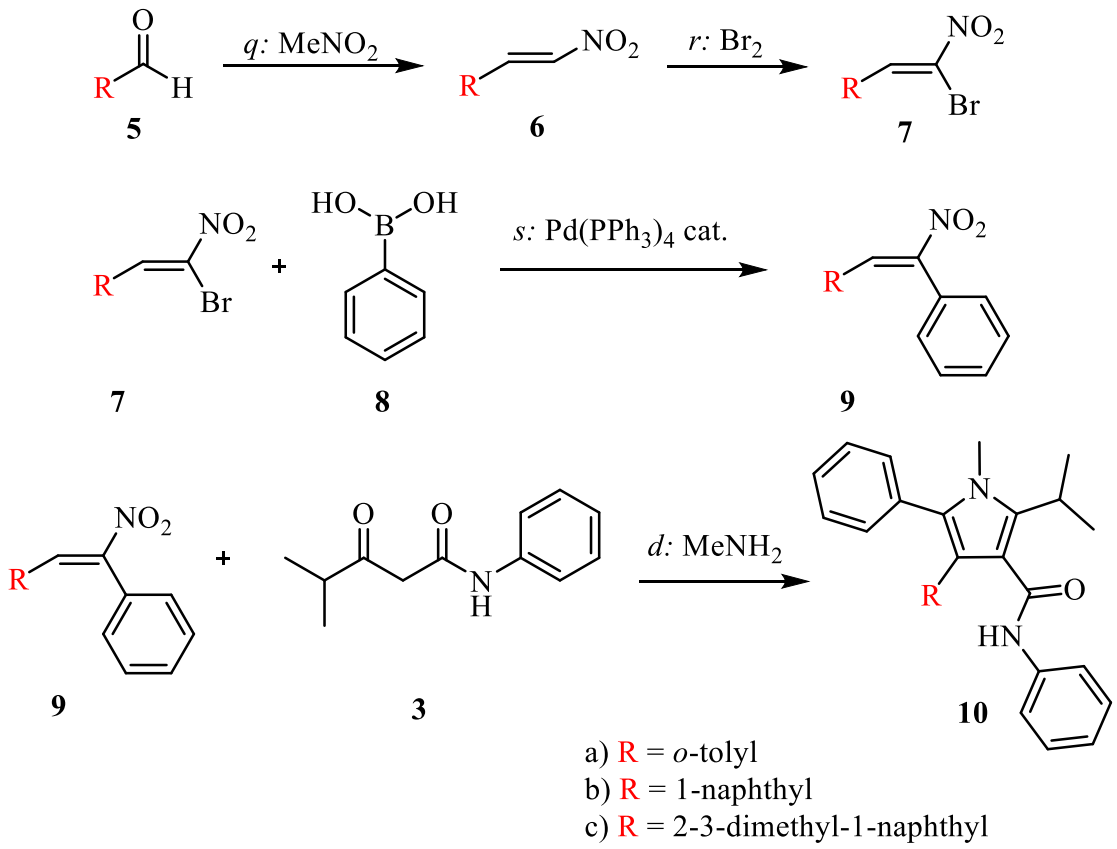

Figure 21 : schematic representation of synthetic pathway II

This way to make the β-nitrostyrene compound **6(a,b,c)**, starts from the aldehyde **5(a,b,c)** by Henry reaction with nitromethane [reaction *q*], to make possible the condensation and the dehydration driven by ammonium acetate [Figure 22]. [27-28-29]

The reaction is conduct using nitromethane as solvent. The excess of $MeNO_2$ can be then distilled out, .and the crude is filtered through silica gel, obtaining the desidered β-nitrostyrene compounds **6** as viscous yellow oils.

Compounds 6 were obtained as a mixture of *E* and *Z* stereoisomers, with the *E* one largely predominating, and they were pure enough to allow to proceed in the synthesis without further purification.

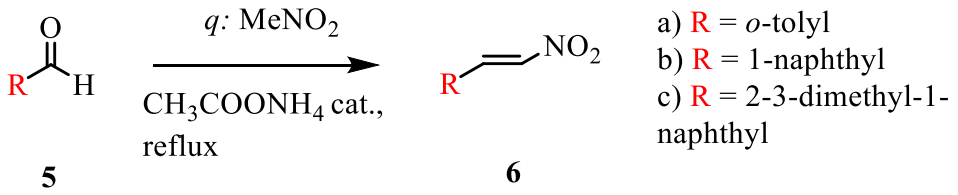

5 **6**

Figure 22 : Henry reaction

The bromination of the alkenes **6** with bromine [reaction *r*] is a reaction that can occur with radical pathway, leading to undesired by-products, The reaction was then carefully protected form the light with aluminium foil.

Compounds **6(a,b,c)** were stirred with sodium acetate in chloroform, paying attention that the temperature does not exceed 0 °C, before adding dropwise the cold liquid bromine solution. If the Br_2 is diluted (1M chloroform solution) is possible to have a better control on the exothermicity of the reaction and to increase the reaction yield.

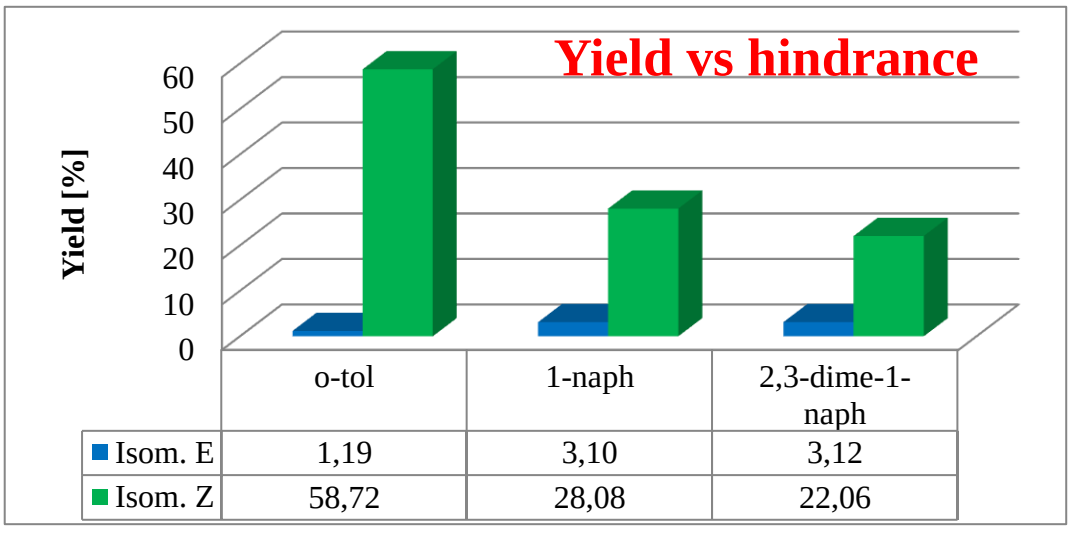

Figure 23: With increasing hindrance, the total yield decrease, and the E-to-Z ratio increase.

The reaction crude contains the *E* and *Z* stereoisomers, and (after the β-elimination the nomenclature is inverted) the yield is lower on increasing the steric size of the aromatic ring (figure 23).[30]

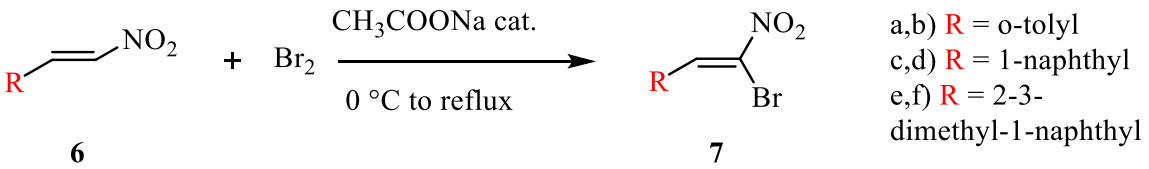

Figure 24: bromination of alkene 6

The main product is the *Z* isomers, but as shown in Figure 23, the ratio *E/Z* is related to the steric hindrance, this because the aromatic compound can fit better in the geometry of the planar nitro group rather than in the larger and spherical electronic cloud of the bromine.

The analysis with ^{1}H-NMR and then with the HPLC show that the reaction produces an noticeable amount of by-product, even if bromination in the desired position is the favourite reaction. In the particular case of the 1-naphathalene ring (and in the 2,3-dimethyl-1-naphthalene substituent) the bromination in para of the aromatic ring is a side reaction that yields double bromination and the wrong attack. [Figure 25]

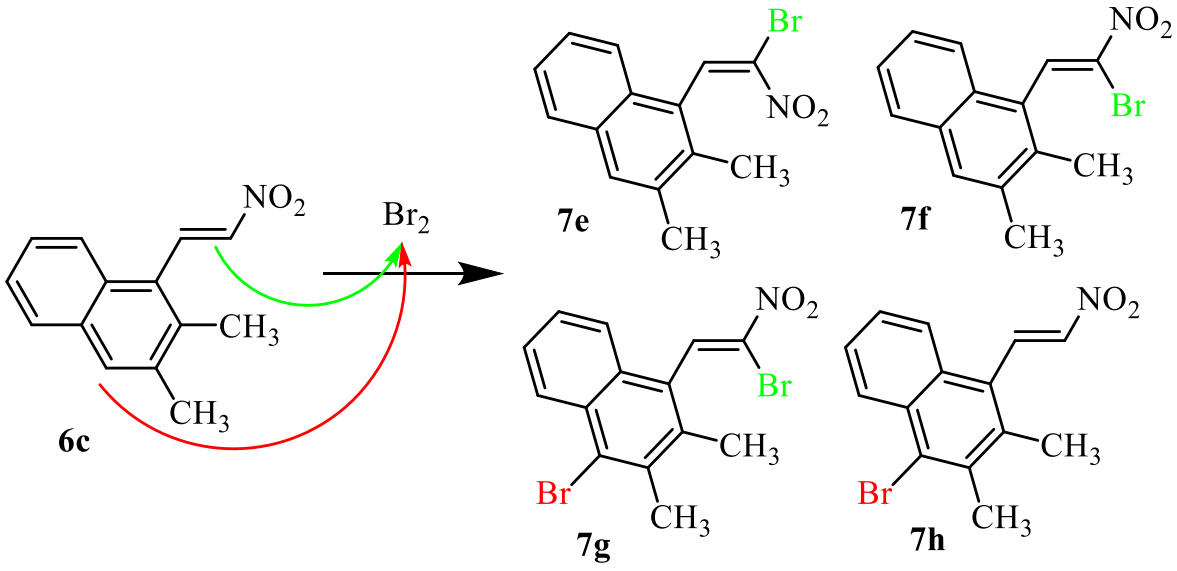

Figure 25: main side reaction, these mechanism are also applied for compound 6b

Unfortunately, the reaction mixture is quite difficult to be resolved, and the three compounds yields very similar NMR spectra. In addition, each compound is a E/Z mixture, and chromatographic separation had to be carefully monitored. The desired

compounds **7c, 7d, 7e** and **7f** were fully identified and characterized by means of NOE and 2D-NMR (HSQC,HMBC and COSY).

When the isomers are purified with HPLC chromatography column, the products are pale yellow oils, the isomers can be collect together.

Compounds **9(a,b,c,d,e,f)** have been synthetized starting from the respective β-bromonitroalkene **7(a,b,c,d,e,f)** through the Suzuki-Miyaura cross-coupling reaction, [31] [32] using tetrakis(triphenylphosphine)palladium(0) as catalyst [reaction *s*]. The reaction products are a mixture of the isomers *E* and *Z* of the phenyl-nitroalkene **9**.

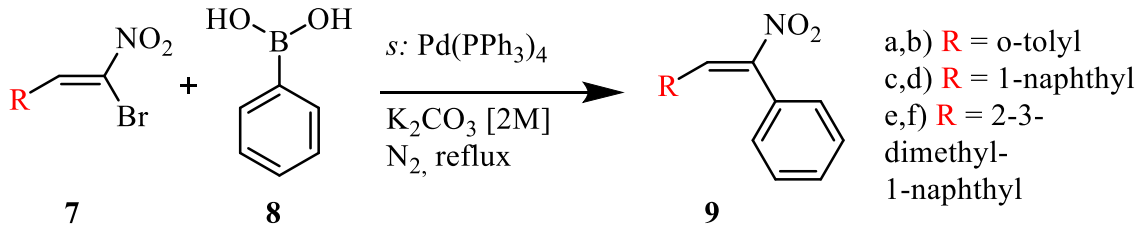

Figure 26: Suzuki-Miyaura coupling reaction with compounds *7* and *8*, to obtain the compounds *9*

The reaction needs to be conduct in absence of oxygen because proceeds the oxidation on the Pd(0) forming the inactive form of PdO. The presence of palladium oxide can be noticed by the formation of a dark suspension. To avoid the deactivation by oxidation is necessary to proceed with the reaction under nitrogen atmosphere and, using a pump, make the solution as much as possible free from the dissolved oxygen.

In the solvent of reaction is dissolved a little amount of cyclopentyl-methyl ether in toluene (1:19 v/v), the reaction is greatly improved, due to its affinity in the activation of boronic acids.[33]

The steric hindrance in position *ortho* did not allow high reaction yields, and, in addition to degradation product is possible to isolate specific by-products such as: the compounds **6** derived from the loss of the bromide group (it is possible to recover it) and the triphenylphosphine obtained from the deterioration of the catalyst.

The boronic acid is added in slight excess and the reaction proceeds until the brominated reagent is converted, or when an early deactivation of the catalyst takes place (usually due to the presence of oxygen in the reaction flask).

The yields of the reaction is very sensitive to the nature of the ortho substituent, and the yield is drastically reduced with the increase in size, favouring the degradation of the reagents. Associated with the low yields of the bromination reaction, this turns out to be a limiting factor of the process and leads to a large quantity of waste produced.

This synthetic pathway has been chosen for the possibility of introducing a chiral catalyst in the last reaction [reaction *d*], the MCR, able to produce an enantiomeric excess. Several tests have been carried out to verify the goodness of the multi-component reaction and it is possible to affirm that, even in the case of low encumbered substituents, the reaction does not proceeds also with the use of achiral catalyst.

Studying the reaction mechanism, we tried to bring it to completion by separating it. The key steps turn out to be: the activation of ethyl 4-methyl-3-oxopentanoate with methylamine to form the enamine (*Z*)-4-methyl-3-(methylamino)-*N*-phenylpent-2-enamide [Figure 27] and the attack of the enamine to the nitroalkene [Figure 28]. These steps create optimal conditions for the cyclocondensation with the NO_2 as leaving group, forming the pyrrole ring.

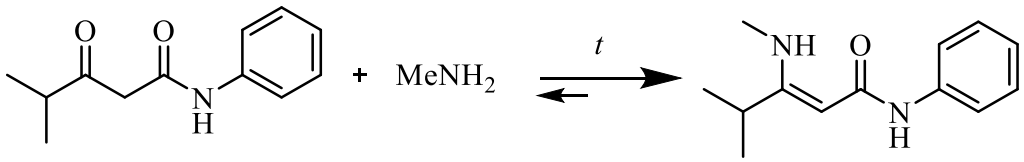

3 **4**

Figure 27: enamine formation

The formation of enamine [reaction *t*] must be conducted with a methylamine solution in ethanol (33% W/W), otherwise the yields very low because of a very low conversion. Following the procedure, instead, product **4** can be obtained with a purity enough to avoid purifications, necessary because the enamine is not very stable and degrades in a short time. The enamine was therefore prepared just before being used (24 – 48 h) and added in ethanol solution to the nitrostilbene.

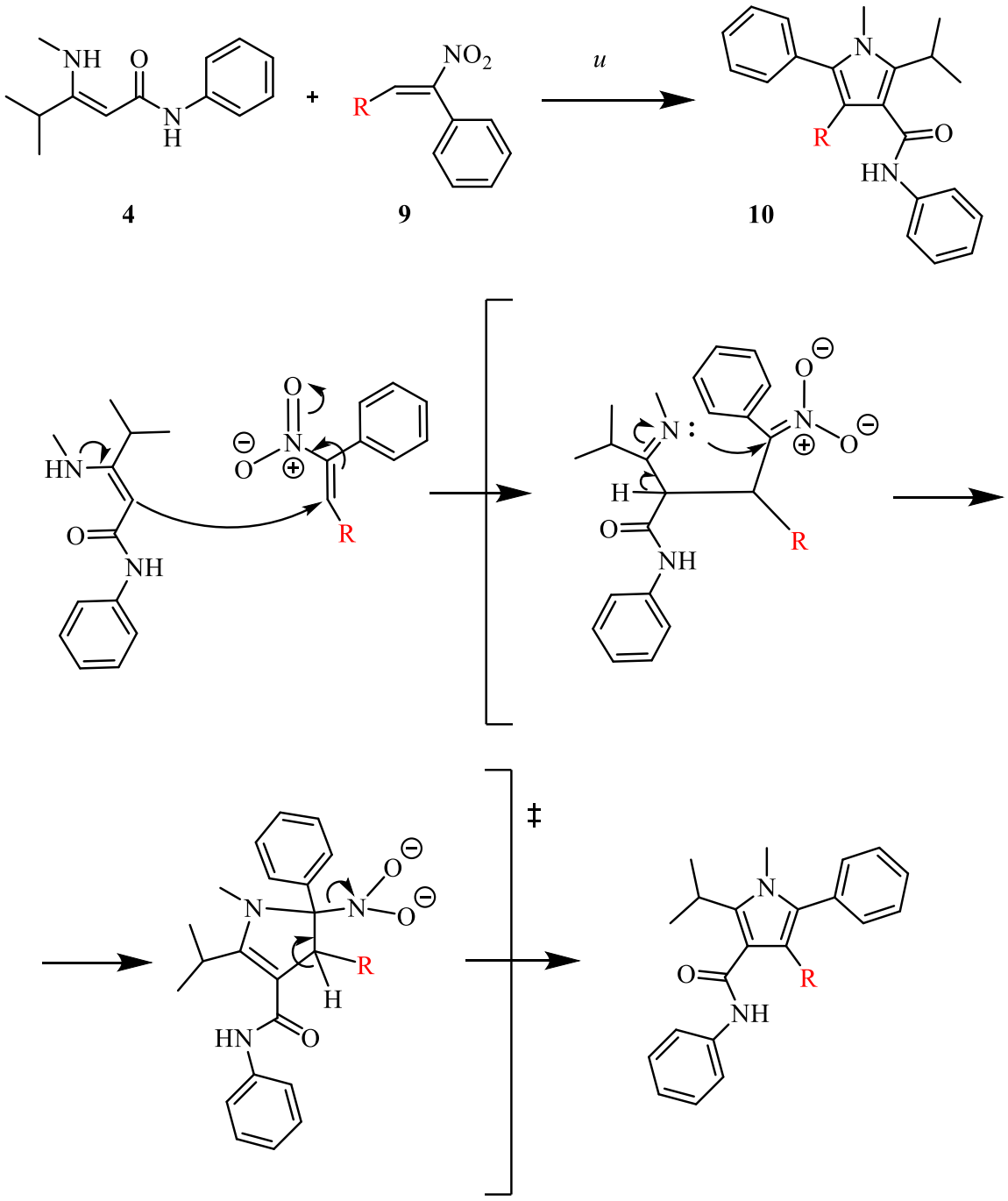

Figure 28: cyclocondensation proposed to form the pyrrole ring

The formation of the pyrrole [reaction *u*] is driven by the presence of the nitro group which is an excellent leaving group, once the enamine attack has occurred, this allows the reaction intermediate to proceed until the cycle is closed. [Figure 28] [34]

The optimal reaction conditions have been defined to be 120 °C in a closed tube for 8 h, producing a low conversion with high selectivity. The conversion, however, turns out to

be a limit because with very hindered nitro-alkenes the closure did not occur even after days of reaction. The products obtained are easily purified by chromatographic column and appears as white solids.

This route of synthesis proved to be able to obtain compound **10a** [2-isopropyl-1-methyl-N,5-diphenyl-4-(*o-tolyl*)-1H-pyrrole-3-carboxamide] and **10b** [2-isopropyl-1-methyl-4-(*naphthalen-1-yl*)-N,5-diphenyl-1H-pyrrole-3-carboxamide] but all the attempts were vain for the synthesis of most hindered **10c** [4-(*2,3-dimethylnaphthalen-1-yl*)-2-isopropyl-1-methyl-N,5-diphenyl-1H-pyrrole-3-carboxamide]. For the synthesis of the last product it was necessary to develop a different synthetic way.

Synthetic pathway III

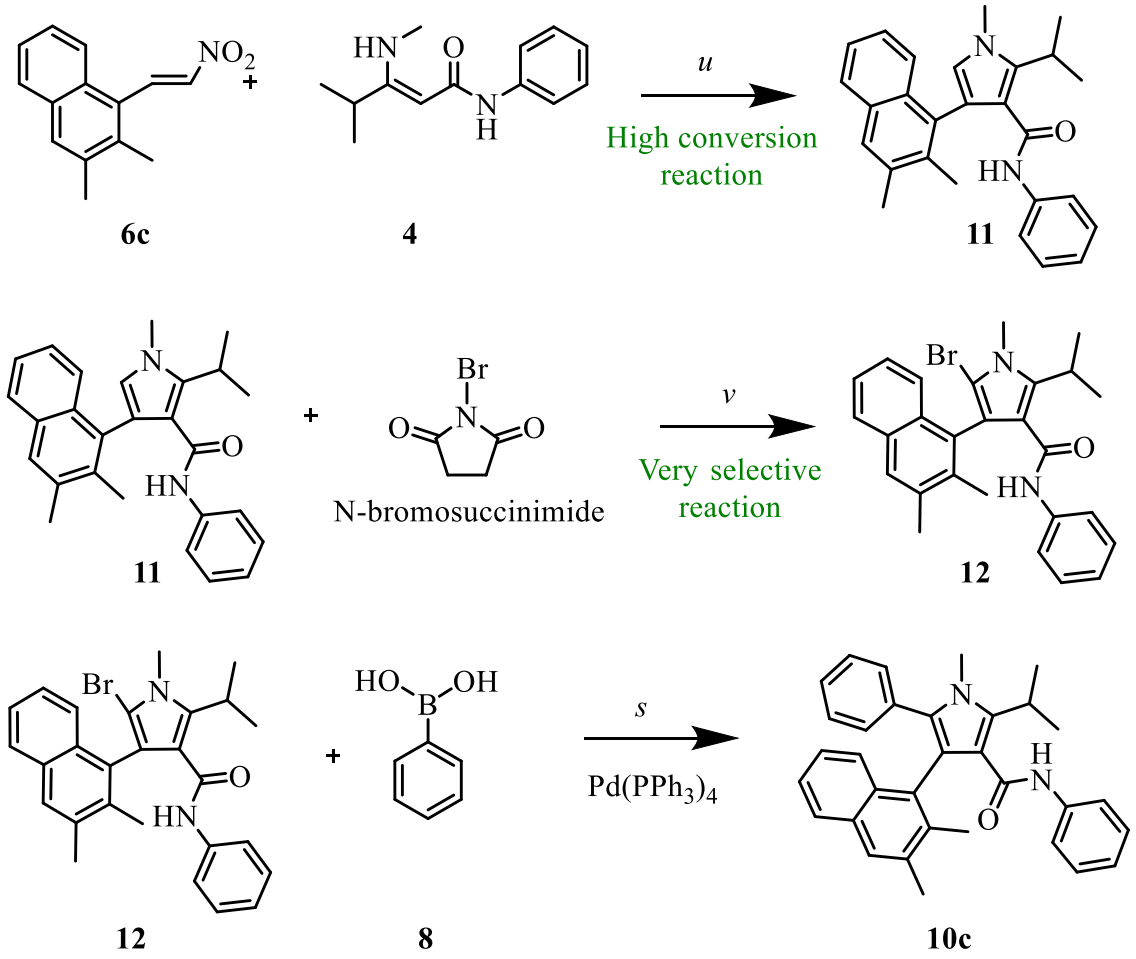

Figure 29: improvements of synthetic pathway II

The new synthetic pathway tries to improve the weakness of the previous ones and to avoid that the steric hindrance may be a limiting factor of the reactions. The new synthesis uses old and new reactions, combined to be more selective and manageable. [Figure 29]

It was decided to proceed as shown above to prepare compound **6c**, then the cyclocondensation reaction was carried on [reaction *u*]. This reaction, with a smaller steric hindrance, yields a better conversion than the previous tests, obtaining the new compound **11** [4-(*2,3-dimethylnaphthalen-1-yl*)-2-isopropyl-1-methyl-N-phenyl-1H-pyrrole-3-carboxamide].

It was argued to develop the closing reaction without the phenyl group for two reasons. At first because it was noted that the phenyl group hampers the nucleophilic attack by nitrogen (before the elimination of the nitro group). Than for the awareness of being able to use N-bromosuccinimide (NBS) to yield the selective bromination on the pyrrole cycle.[35]

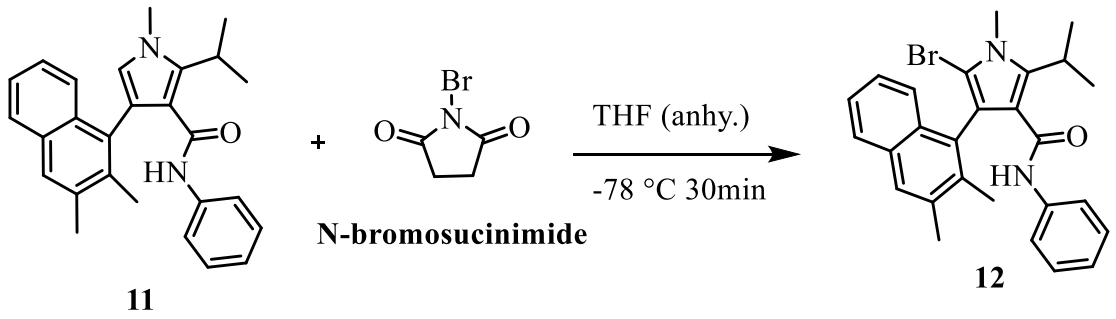

Figure 30: Bromination with NBS

Br_2 cannot be used in this reaction because the consecutive reaction is the bromination in position 4 of the naphthalene. [Figure 30] The reaction with NBS smoothly proceed under anhydrous conditions and at -78 °C, with almost quantitative yields. The product can be purified on silica gel, as a white solid.

The final molecule was obtained using phenylboronic acid and the Suzuki-Miyaura coupling. The reaction is carried out under the same condition described above, with yields above 70%.

In this new synthetic method the purification of the final product is easy, it was obtained much higher yields due to the less influence by the substituent in position 3. In addition

to that, it will be simple to use the 4-fluorophenylboronic acid in the preparation of the final atorvastatine.

An enantioselective synthesis could still be devised using a chiral catalyst in the Suzuki reaction, but has not been analysed in this study.

The overall yields for the 4-step synthesis was 12% when pathway III was used, whereas the yields were lower in the case of pathway II (6.3% for compound **10b** and 2% for compound **10a**).

3.2. Conformational studies

A pair of atropisomers is obtained with different asymmetric aromatic groups bonded to the pyrrole scaffold, because the aryl ring is displaced out of the plane, and the presence of the ortho substituent yields a stereogenic axis. Thanks to the 180° rotation around this axis, we can switch from one atropisomer to the other [Figure 31]. The stability of these conformational isomers depends on the steric hindrance of the ortho substituent, due to the electronic repulsion with the electronic clouds of the other molecular fragments (phenyl group in position 2 and amide group in position 4). If there is a large steric hindrance, the two atropisomers will also be thermally stable at room temperature.

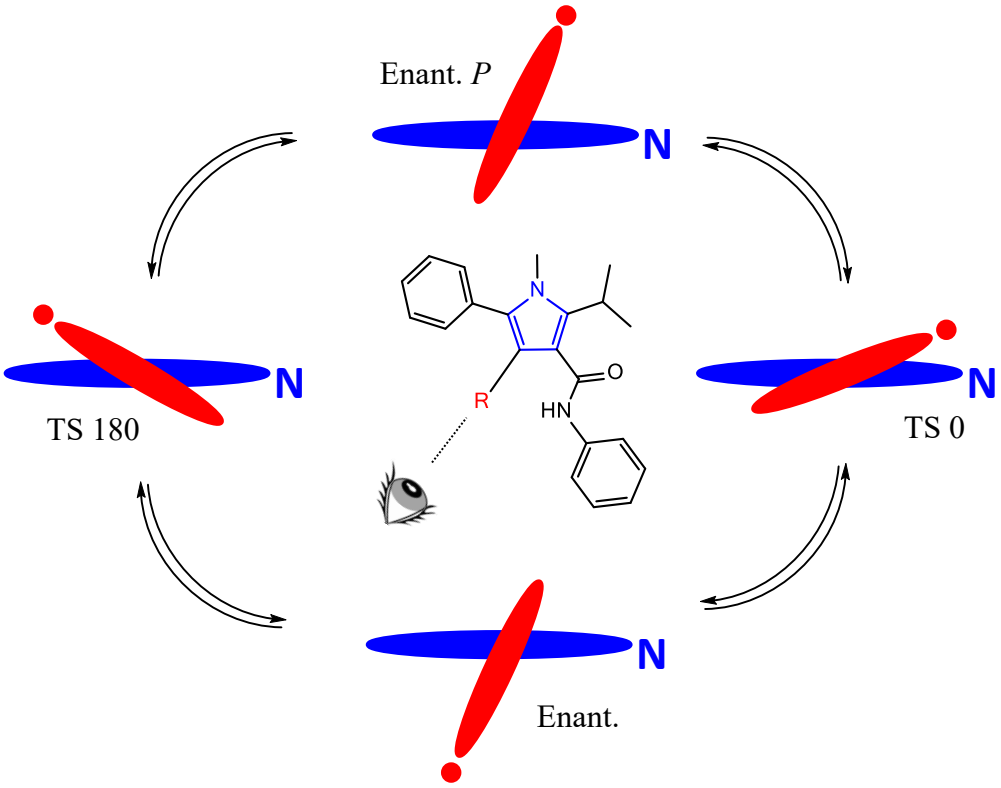

Figure 31: schematic example of a racemization process of an atropisomer, during the racemization the transition states are reached.

To investigate if the conformations will be thermally stable or not we can calculate the rotational energy barrier by DFT methods.

10a) 2-isopropyl-1-methyl-*N*,5-diphenyl-4-(*o*-tolyl)-1H-pyrrole-3-carboxamide

DFT calculations were used to determine the most stable conformations of the compound. Through the calculations we have obtained the energies related to the ground state (GS) and those related to the transition state geometries. The GS obtained are 4, and they show very small differences in energy among them, so they can all be assumed being populated. All configurations refer to the M enantiomer, and differ in energy due to the different positions of the substituents. [Figure 32]

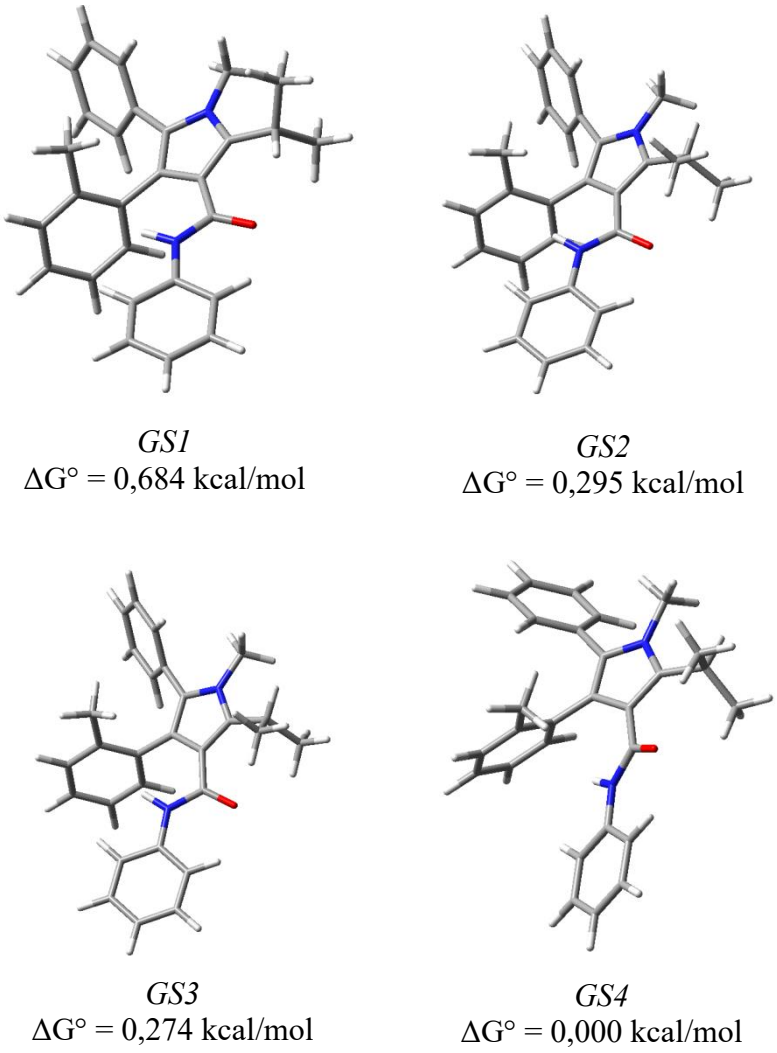

Figure 32: fundamental state geometries resulting from DFT calculations

The geometries of the transition states (TSs) represent the maximum energy during the racemization between the two enantiomers. During this process the substituent is moved into a planar position with respect to the pyrrole ring, forcing to bend and to deform in order to minimize the energy. Two TSs were hypothesized for racemization; TS 0 where the methyl rotates towards the phenyl group, and the TS 180 where the methyl rotates towards the amide group. [Figure 33]

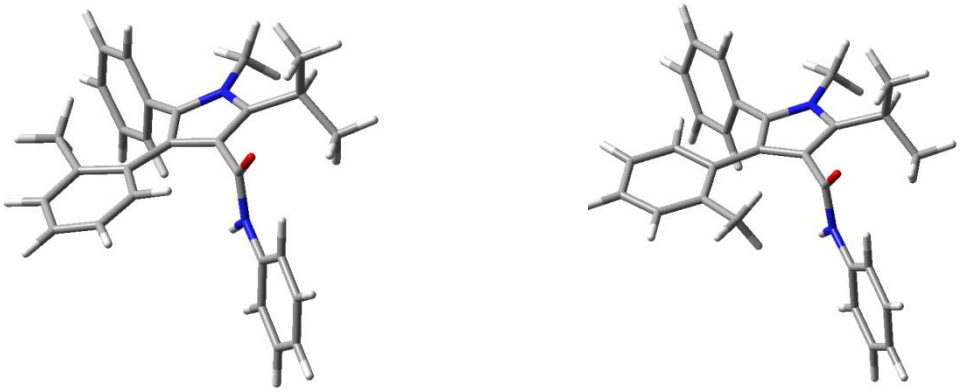

TS 0
$\Delta G^{\ddagger}$ = 23,564 kcal/mol

TS 180
$\Delta G^{\ddagger}$ = 23,320 kcal/mol

Figure 33: optimized geometries fo the TSs

The data obtained from the calculations remains an indication, it is necessary to experimentally verify the values of the rotation energy. Having obtained a prediction of about 23 kcal/mol, it was feasible to perform the analysis with a variable temperature NMR spectroscopy (VT-NMR).

Within the molecule the *i*-propyl group is present; this is a diastereotopic group that has the particularity of splitting its own NMR signals when it is in a chiral environment, these groups area usually defined *chiral probes*.

In atropisomeric molecules, the *i*-propyl group will show different multiplicity when the two methyl groups occupy positions with a different magnetic environment longer than the NMR acquisition times. Therefore, when the rotation of the chiral axis is slower slower than the acquisition times, the peaks relative to the two methyls of the isopropyl group yield different chemical shift.

During the VT-NMR experiments, the behaviour of the methyl peaks varies according to the temperature. Acquiring a temperature that allows a slow rotation, the signals give two doublets with a different chemical shift. Increasing gradually the temperature, the rotation around the chiral axis will broad the two signas until the coalescence temperature is reached. Once the temperature is further increased, the rotation of the asymmetric substituent will be faster than the NMR acquisition times, showing a single signal.

In the case of **10a**, two methyl peaks were observed around 1,52ppm (^{1}H-NMR , 600MHz, $C_2D_2Cl_4$) where the two different doublets can be distinguished up to +103 °C, Above this temperature the coalescence of the peaks is reached and only one doublet is observed.

Thanks to the line shape simulation of the VT-NMR spectra, it is possible to obtain, through mathematical models, the kinetic constants of the dynamic processes and therefore the $\Delta G^{\ddagger}$. The program used for the simulation is the DNMR-6 QPCE No. 633 (Dynamic Nuclear Magnetic Resonance - Quantum Chemistry Program Exchange). The program can simulate theoretical NMR spectra according to the change of the kinetic constant and so it is possible to compare them to the experimental ones, obtaining the $\Delta G^{\neq}$ at different temperatures.

Figure 34 compares the results obtained experimentally as the temperature changes and the corresponding simulations as the *k* changes. The theoretic energy is given by the average of the simulated energies

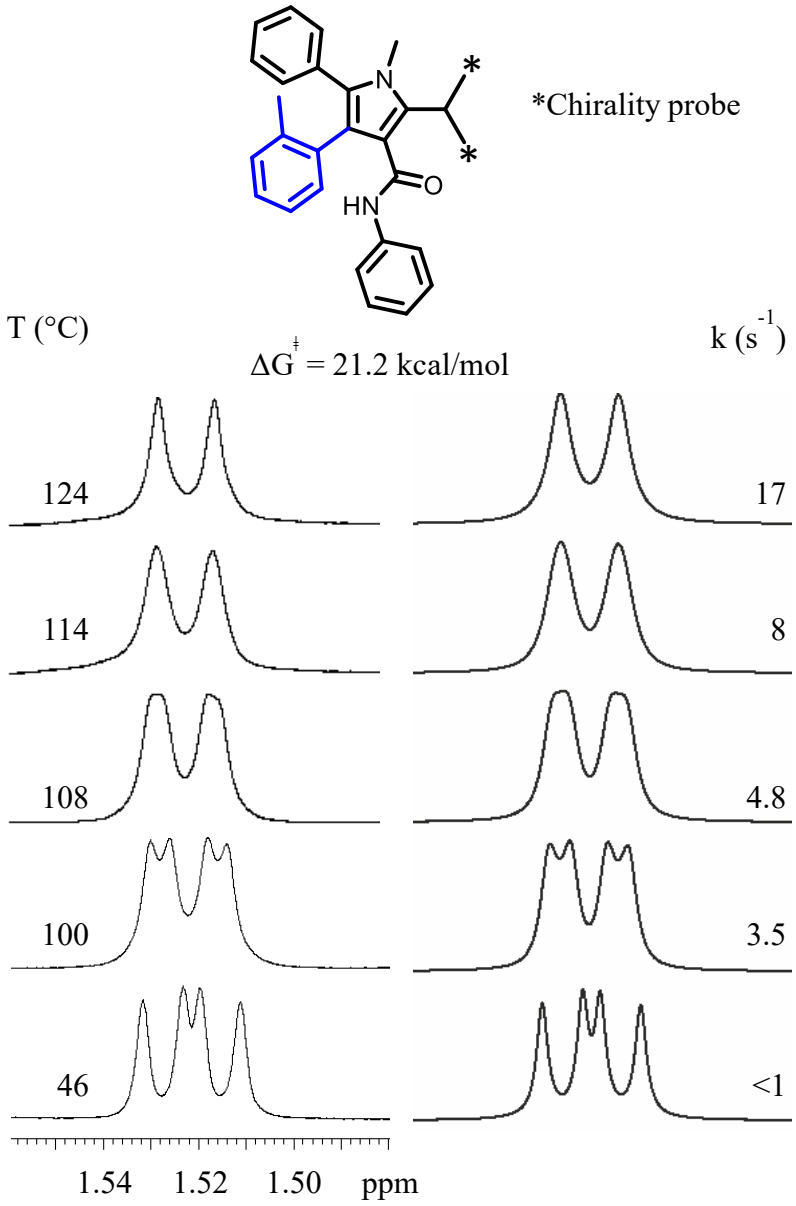

Figure 34: summary of the VT-NMR study where, on the left is shown the trend of the chirality probe peaks as a function of temperature, while on the right the line shape simulation is shown, highlighting the value of k.

For the molecule **10a**, the rotational barrier energy was determined by the Eyring equation to be 21.2 kcal/mol, a value that agree well with that predicted by the DFT calculations. Compounds **10a** has a half-life time at +25 ° C of 392.5 s ($k = 1.77*10^{-3}$ s^{-1}). It falls into class 2a of the LaPlante classification.

10b) 2-isopropyl-1-methyl-4-(naphthalen-1-yl)-N,5-diphenyl-1H-pyrrole-3-carboxamide

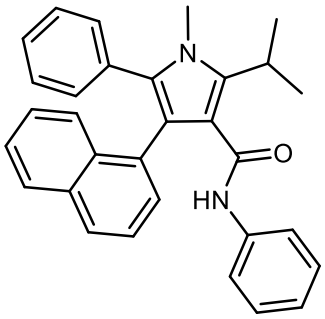

Compound **10b** has as substituent in position 3 the 1-naphthyl group, designed to increase the energy related to TSs and to raise the rotational energy barrier.

Initially, the GSs were identified using DFT computational calculations. [Figure 35] Unlike compound **10a**, only 3 GS can be defined as populated for molecule **10b**, because the combination of the gearing of the aryl ring and the amide yield a large steric hindrance with the *i*-propyl when its H is directed towards the amide group..

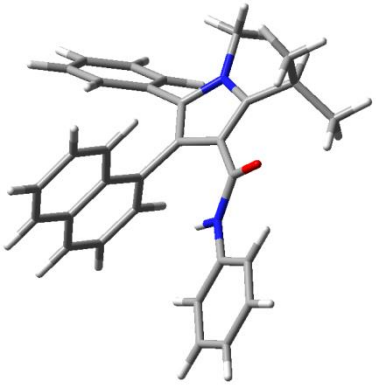

GS1
ΔG° = 0,000 kcal/mol

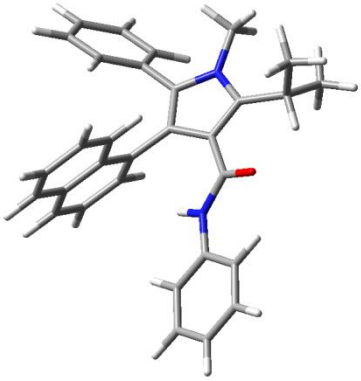

GS2
ΔG° = 0,484 kcal/mol

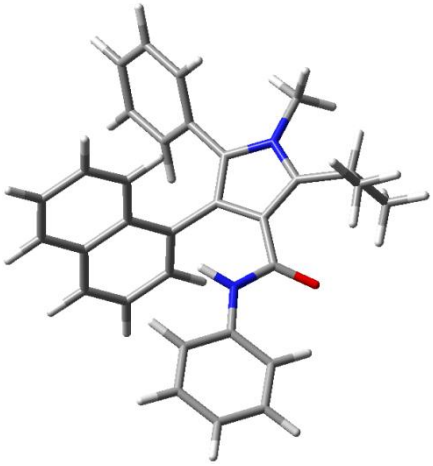

GS3
ΔG° = 0,754 kcal/mol

Figure 35: fundamental state geometries resulting from DFT calculations

After having determined the GSs conformations, we proceed with the calculation of the geometries related to the TSs. Two conformations have been hypothesized corresponding to the two different movements necessary for racemization and have been optimized through DFT calculations. [Figure 36]

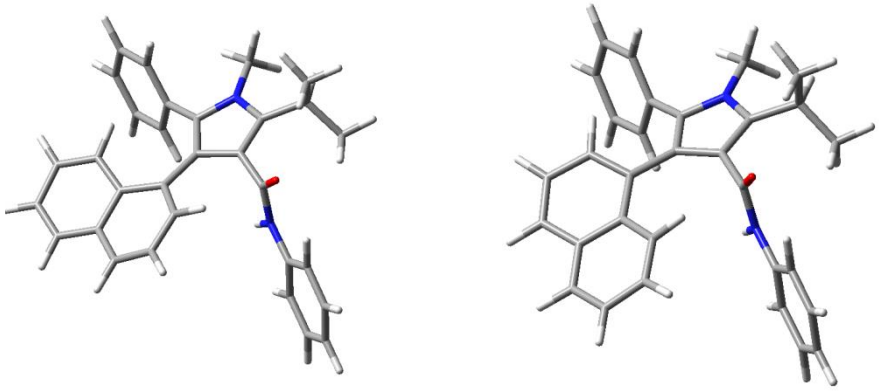

TS 0
$\Delta G^{\ddagger}$ = 24,463 kcal/mol

TS 180
$\Delta G^{\ddagger}$ = 24,960 kcal/mol

Figure 36: optimized geometries fo the TSs

Calculations suggested a rotational barrier energy of about 24 kcal/mol; this barrier cannot be analysed by VT-NMR, but the atropisomers can be analyzed by HPLC.

Using an HPLC equipped with a chiral column, it is possible to separate a mixture of enantiomers thanks to the different interactions with the enantiopure stationary phase. In the case of atropisomers with a rotation energy between 21-23 kcal/mol, the resolution and interconversion of the enantiomers occur simultaneously within the column, showing a characteristic chromatogram showing a plateau between the two peaks relative to the enantiomers. This technique is called Dynamic-HPLC (D-DPLC)

During the D-HPLC analyses, chromatograms of the racemic atropisomer compound are recorded at different temperatures. By gradually increasing the temperature, more energy is supplied to the system and the racemization is faster, thus showing an increase in the intensity of the plateau. The limit is obtained when the racemization is faster than the separation, leading to the coalescence of the peaks.

Similarly to VT-NMR, the kinetic constants are determined by the line shape simulation of the experimentally obtained chromatograms but in this case the equilibrium of the atropisomers is a dynamic system and therefore it is necessary to use the stochastic (time-

dependent) method for the simulation of the chromatograms. The result of the simulation is expressed through two energies because the equilibrium of the enantiomers is represented through the kinetic constants k_{1-2} referring to the conversion of 1 in 2 and the constant k_{2-1} referring to the inverse reaction.

The molecule **10b** was analysed at temperatures of +35, +40, +45 °C using the chiral column ChiralPack AD-H with eluent hexane:$_i$-propanol 80:20 and flow 1 ml/min. [Figure 37]

$k_{1-2} = 1.06*10^{-3}\ s^{-1}$ and $k_{2-1} = 5.41*10^{-4}\ s^{-1}$ are determined by the simulations, by solving the Eyring equation, $\Delta G^{\ddagger}_{1-2} = 21.5$ kcal/mol and $\Delta G^{\ddagger}_{2\ -1} = 21.9$ kcal/mol is attributed to the compound, this defines a half-life time that is between 650 and 1300 s.

The difference between the experimental and the calculated energy is part of the error associated with DFT calculations, especially for molecules that show a strong correlatated motion among the movements of the different substituents.

Compound **10b**) belongs to the class 2a of the LaPlante classification and is not yet a stable atropisomer.

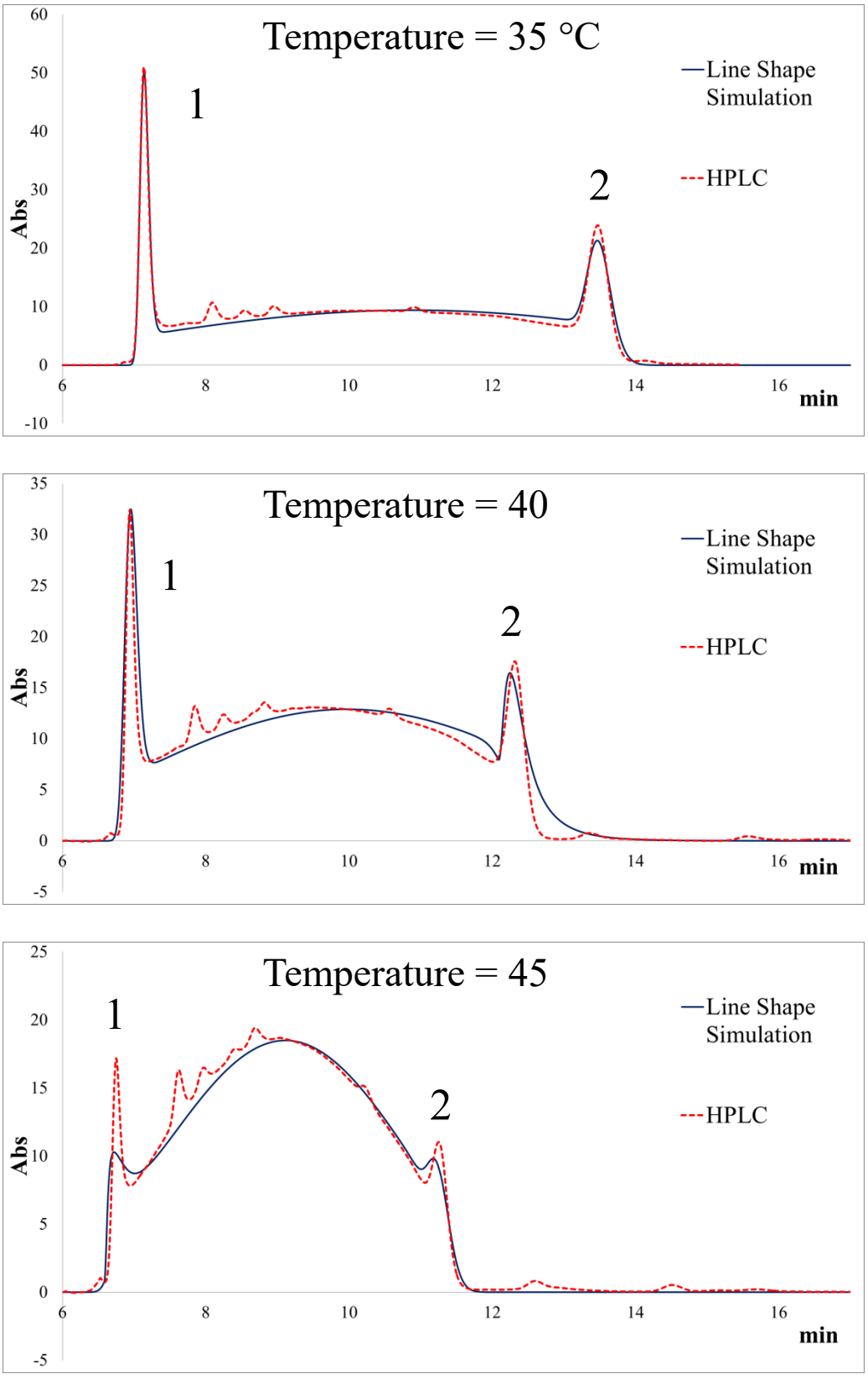

Figure 37: overlap of the D-HPLC chromatogram with those obtained from the simulation for the calculation of ΔG‡

10c) 4-(2,3-dimethylnaphthalen-1-yl)-2-isopropyl-1-methyl-N,5-diphenyl-1H-pyrrole-3-carboxamide

In order to further increase the steric hindrance of the substituent in position 3, the synthesis with 2,3 diMe-1-naphthalene group was designed, so the racemization process was further encumbered by the methyl groups.

The GS geometries were analysed by DFT calculations. As for compound **10b**, only 3 GSs were populated because of the large encumbrance of the substituent in position 3. The large size of the 2,3-dimethylnaphthyl substituent reduces the possibility of populating geometries, and one in particular (GS4) is strongly favoured. [Figure 38]

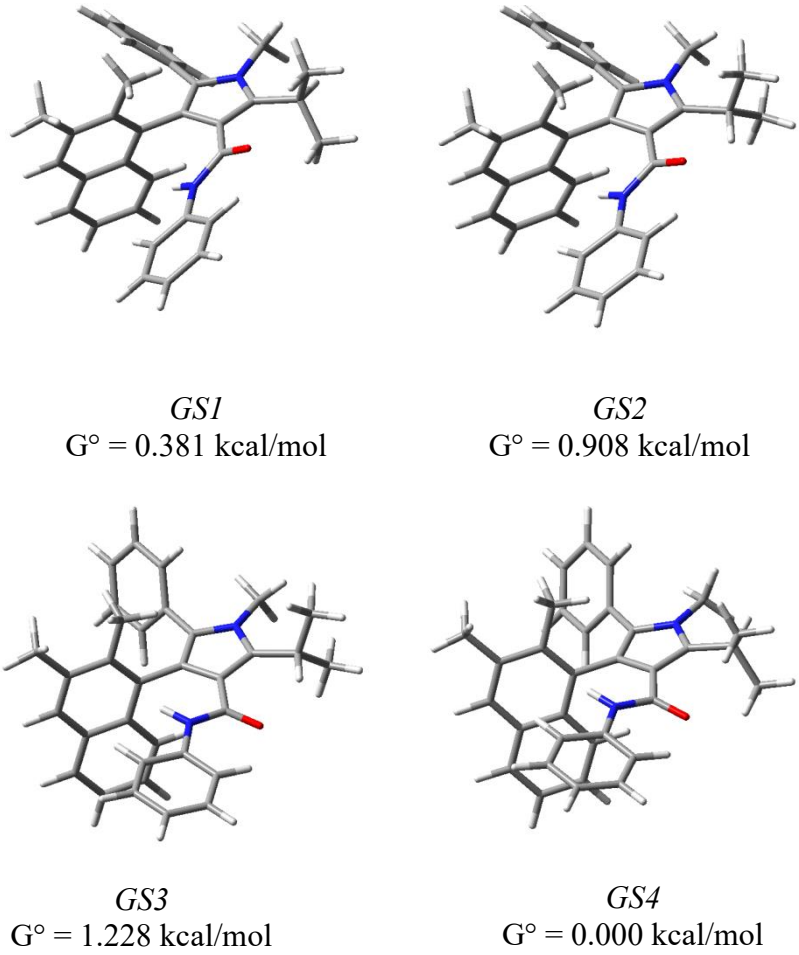

Figure 38: fundamental state geometries resulting from DFT calculations

By determining the energies associated to the GS, it is possible to proceed with the analysis of the relative energies of the TS through the optimizations of the geometries. The calculation suggests a rotational barrier of about 37 kcal/mol and therefore it is feasible to proceed with kinetic studies for the determination of the rotational barrier. [Figure 39]

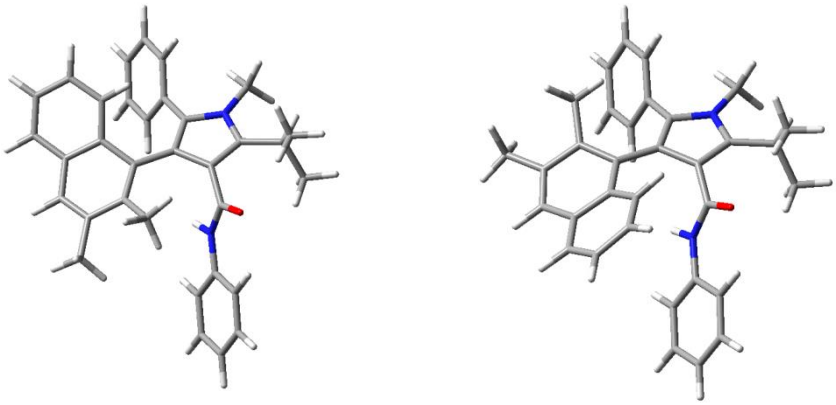

TS 0
$\Delta G^{\ddagger}$ = 37,687 kcal/mol

TS 180
$\Delta G^{\ddagger}$ = 37,740 kcal/mol

Figure 39: optimized geometries fo the TSs

From these images, the bending of the substituent in position 3 can easily be noticed, as well as the modification of the whole molecule during the racemization process.

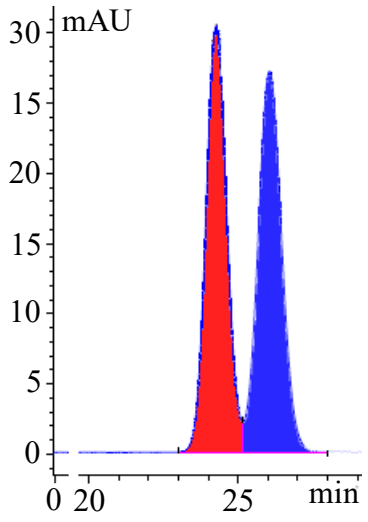

Figure 40: elution condition in analytical HPLC AD-H, 95:5 hexane/IPA, 1 ml/min, 25 °C. The second images shows the superimposition of the spectra of the two enantiomers.

Before proceeding to the kinetic studies, it was necessary to separate the enantiomers to obtain a totally pure one, the separation was made with preparative HPLC using the chiral ChiralPack AD-H column, with eluent hexane:*i*-propanol 85:15, flow 20 ml/min at a temperature of +25 °C. Once eluted from the column, separated enantiomers were collected in ice-cooled flasks and kept in the freezer at -24 °C until the next analyses. [Figure 40]

Kinetic analyses are carried out on racemization as in the case where there is a first order reaction. The enantiomerically pure solution is heated to arbitrary temperatures, selected to observe the racemization, at determined intervals a sample of the solution is taken

and then stored in an ice bath to interrupt the active processes. The different samples are then analysed in HPLC to verify the enantiomeric excess

Due to the high thermal stability of **10c**, the degradation was obtained before racemization during the analysis. The HPLC chromatogram of the compound heated to 146 °C shows a 4.5% racemization after 23 hours. [Figure 41]

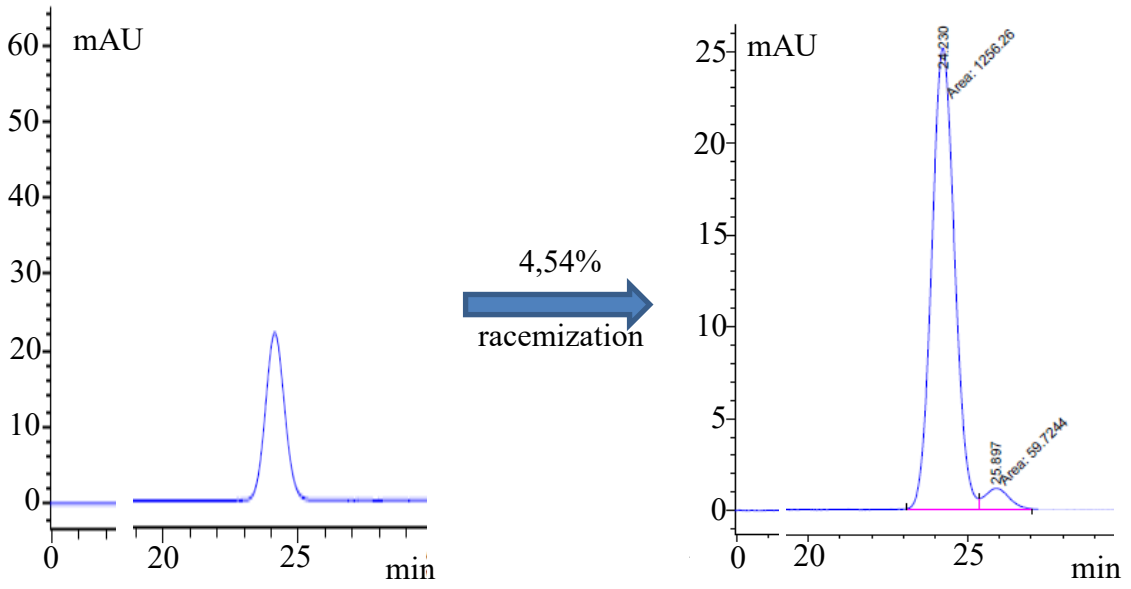

Figure 41: HPLC chromatograms obtained from samples for kinetic analysis.

For practical reasons, no better results could be obtained but the data could be analysed anyway. The kinetic constant is extrapolated from the equation:

$$\ln(x_{eq} - x) = -2k_{(T)}\, t + ln\, x_{eq} \qquad 1.1$$

where x is the molar fraction of the emerging compound while x_{eq} is the molar fraction at equilibrium (x_{eq} = 0.5).

Plotting ln(x_{eq}-x) with respect to time (t), the kinetic constant can be obtained by analysing the slope of the resulting straight line evaluated as $6.99*10^{-15}$ s^{-1}, then solving the Eyiring equation the barrier energy $\Delta G^{\ddagger}$ = 36.7 kcal/mol can be determined.

The compound is stable according to the classification of LaPlante (class 3) and a half-life time of thousands of years has been calculated ($9.92*10^{13}$ s) at a temperature of +25 °C.

3.3. Analysis of the absolute configuration

Having the possibility of obtaining a pure stable enantiomer of the compound **10c** , the absolute conformation was analysed. The two peaks deriving from the HPLC separation were analysed separately using electronic circular dichroism (ECD). A JASCO J-810 spectropolarimeter was used and the sample was dissolved in a HPLC-grade acetonitrile solution. The concentration was about $1 \cdot 10^{-4}$ M, optimized in order to have a maximum absorbance between 1 and 1.2 (UV/vis), with a cell path of 0.2 cm. The spectrum was obtained by the sum of 8 scans at 50 nm·min^{-1} scan rate. [Figure 42]

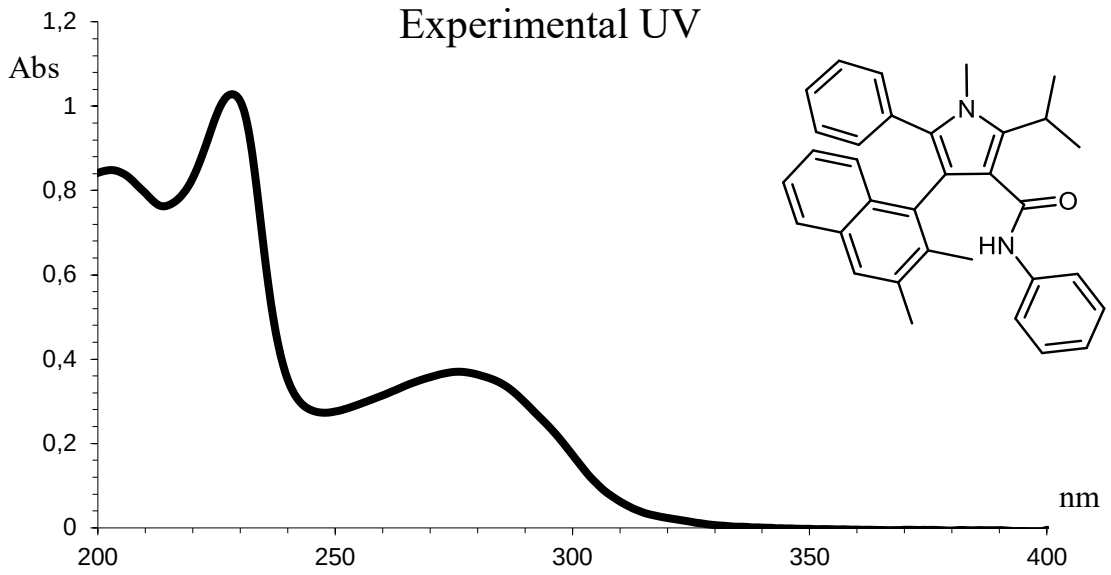

Figure 42: UV-Vis spectrum of the compound 10c analysed from 200 to 400 nm.

The molecule shows an absorption peak around 233 nm due to the presence of numerous π systems of the aromatic groups.

ECD analysis is possible because the Chiral molecules exhibit circular birefringence, which means a solution of a chiral substance through which right circular polarized light and left polarized light (R-CPL and L-CPL) are propagated at different speeds. On the circularly birefringent medium, the phase relation between the circularly polarized lights and the resultant linearly polarized wave rotates. This is the origin of the phenomenon known as optical rotation.

The CD signal is composed by the difference: CD = A^L - A^R, in other words the difference between the absorbance of left and right circular polarized light. Usually it is expressed in the difference of molar attenuation coefficient for the L-and R-CPL of the

chiral media: $\Delta\varepsilon = \varepsilon^{L} - \varepsilon^{R} = \frac{CD}{c\,l}$ because it is independent by the concentration (*c*)and the path length (*l*).

Analytical quantity of pure enantiomers are separated, allowing to obtain ECD charts. [Figure 43]

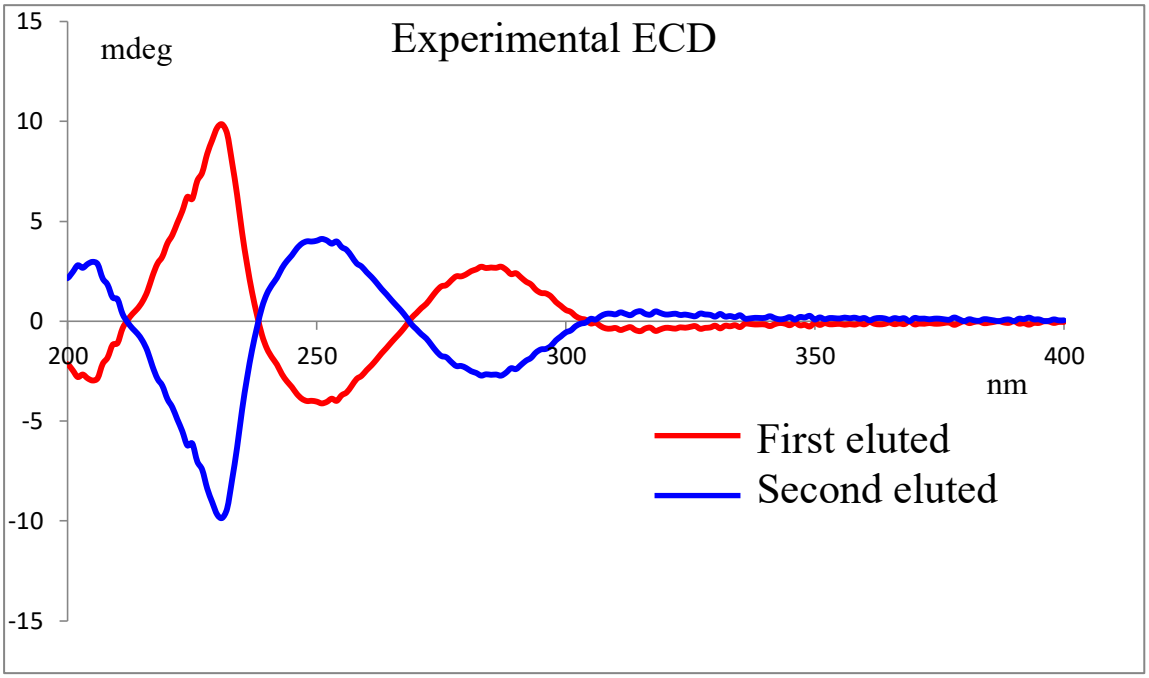

Figure 43: Experimental ECD spectra of the two atropisomers of 10c.

To determine the absolute conformation of the enantiomers, it is necessary to compare the experimental ECD spectrum with the one calculated using time-dependent DFT calculations. This is an extension of DFT where the conceptual and computational foundations are analogous and it adds the possibility to consider the proprieties of many-body system in the presence of time-dependent potentials, such as electric or magnetic fields.

The theoretical ECD spectra of all optimized ground state conformations were obtained with various functionals and the 6-311++g(2d,p) bases set. The most common functionals are hybrid ones such as BH&HLYP, M06-2X, ωB97XD, which includes empirical dispersion and CAM-B3LYP which includes long range correction using the Coulomb Attenuating Method.

Figure 44 shows the simulated ECD spectra with different functionalities of the 4 GS associated with the compound **10c** as M enantiomer:

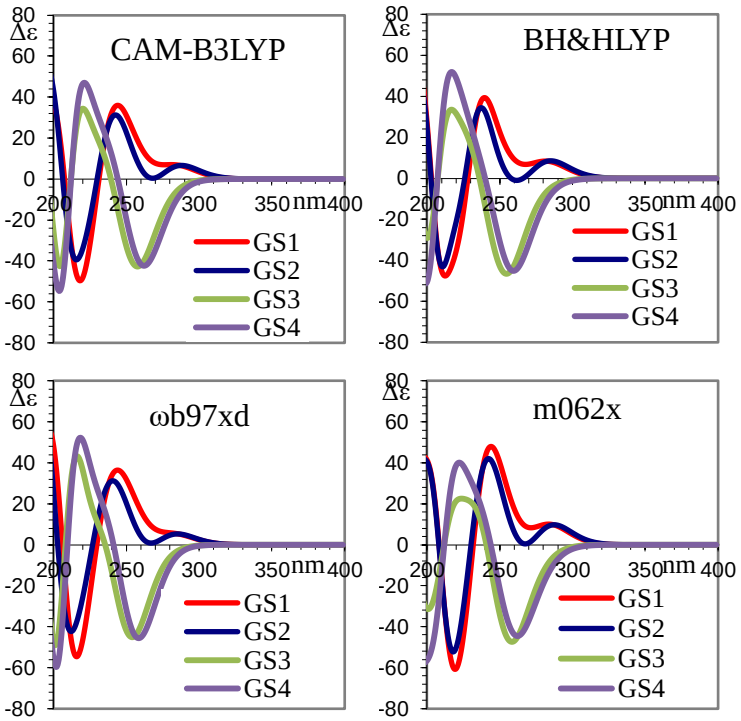

Figure 44: calculated UV-vis spectra related to the possible GS, the calculations were condotticon different functional to obtain comparable results

The experimental ECD spectrum is determined by linear combination of ECD spectra of each conformation weighted by their Boltzmann distribution (coloured line) then it is compared with the experimental one (black line). In order to obtain a better overlap, the spectra were red shifted by 20 nm and multiplied by a factor 0.2 for CAM-B3LYP, BH & HLYP, ωB97XD while it was red shifted by 15 nm and scaled by 0.16 for m062X. [Figure 45]

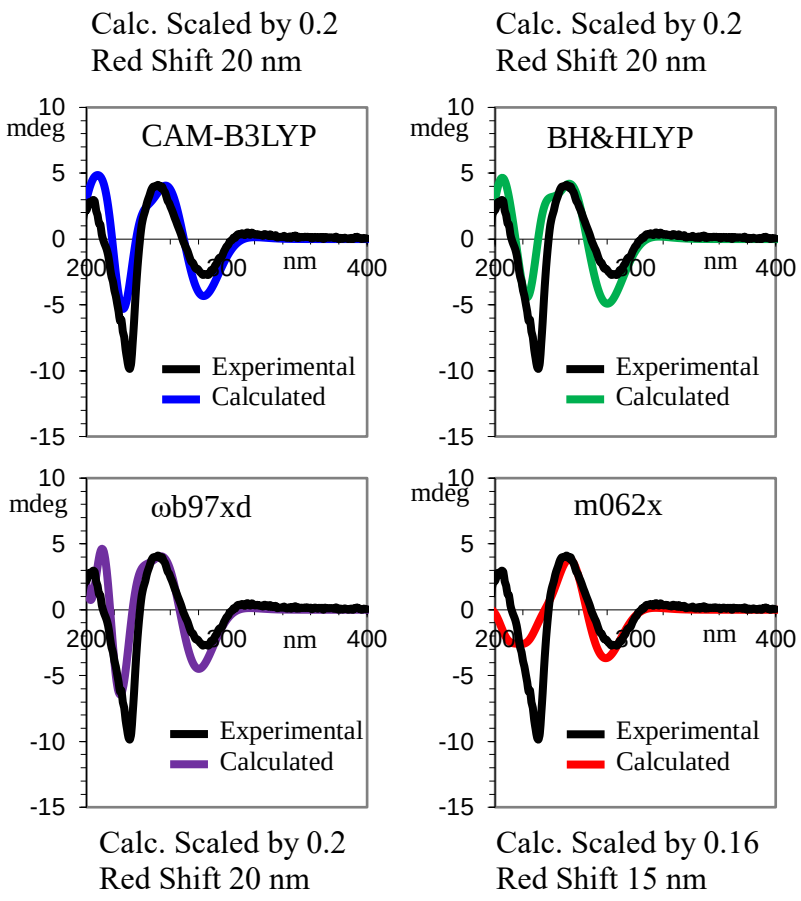

Figure 45: the calculated spectra for the different GS have been added together to have a graph comparable with the experimental spectra

The TD-DFT simulation for the M atropisomer fits very well with the experimental ECD spectrum of the second HPLC eluted **10c** except in the case of the M06-2X functional which can hardly simulate the 230 nm band. This convergence of the data is a good result of the whole stereochemical assignment, therefore the second eluted has M as configuration, while the first one has P as configuration.

4. Conclusions

A convenient synthetic pathway for the preparation of the core structure of atorvastatine has been designed and optimized, with overall yields of 12% over four steps. The synthesis allow to insert different, asymmetric, aryl rings in position 3 of the pyrrole, thus generating a stereogenic axis.

In the case of o-tolyl and 1-naphthyl aryl rings (compounds **10a** and **10b**), the atropisomers are stereolabile, and their racemization barriers (21.2 and 21.5 kcal/mol, respectively) have been measured by dynamic NMR and Dynamic HPLC.

In the case of the most hindered aromatic system (2,3-dimethylnaphthyl, compound **10c**), the racemization barrier was found to be sufficiently high to allow for the physical resolution of the atropisomeric pair on an enantioselective HPLC column. The racemization barrier was estimated as 37.7 kcal/mol by monitoring the racemization rate by HPLC.

The absolute configuration of the two atropisomers of **10c** has been assigned by means of theoretical simulation of the Circular Dichroism spectra using TD-DFT simulation.

5. Experimental section

5.1. Materials

The commercially available reagents used are: 4-methyl-3-oxopentanoate; aniline; acetic acid; sodium bicarbonate; hydrochloric acid; sodium chloride; methylamine (33%^{w} in ethanol); 2-methylbenzaldehyde; 1-naphthaldeyde; ammonium acetate; nitromethane; sodium acetate; bromine; phenylboronic acid; potassium carbonate; tetrakis(triphenylphosphine)palladium(0); N-bromosuccinimide.

The solvent used are: toluene; hexane; ethanol; petroleum ether; dichloromethane; chloroform; CPME; ethyl acetate; demineralized water; THF anhydrous Deuterated solvents for NMR spectra are commercially available.

5.2. Instruments

The stationary phase used for the chromatographic column is composed of 60 Å Silica gel (230-400 mesh, Sigma Aldrich) suitable for flash chromatography column. Silica gel plates 60 F254 (Merck) were used for the TLCs. Reactions requiring anhydrous conditions are made under nitrogen flow (inert atmosphere). The glassware used in these conditions was prepared by heating it to +70 °C at least three hours before the reaction.

The Waters 600 HPLC with a wavelength set at 254 nm was used to purify the products. The columns used are described in the product characterizations.

The ^{1}HNMR, ^{13}C-NMR spectra were recorded with Varian Inova 600 MHz, Varian Mercury 400 MHz and Varian Gemini 300 MHz spectrometers. The chemical shifts are given in ppm relative to the internal tetramethylsilane standard (^{1}H and ^{13}C) or relative to the peak of the residual solvent. The assignment of the multiplicity of the carbons is obtained by means of the DEPT sequence.

Tests conducted in NMR at elevated temperatures have been possible through an electrical resistance inside the instrument, inside the probe a Cu/Ni thermocouple measures and regulates the temperature so that it remains fixed. The temperature calibration is done using a digital thermometer and the thermocouple. Then, a calibration line is needed because the temperature is not measured throughout the probe. In fact, there will be variations with respect to the base, where I have the thermocouple and the

upper part where there is placed. The measurement uncertainty can be estimated around ± 1 °C.

5.3. Synthesis and characterisation

*4-methyl-3-oxo-N-phenylpentanamide 124401-38-3 [**3**]*

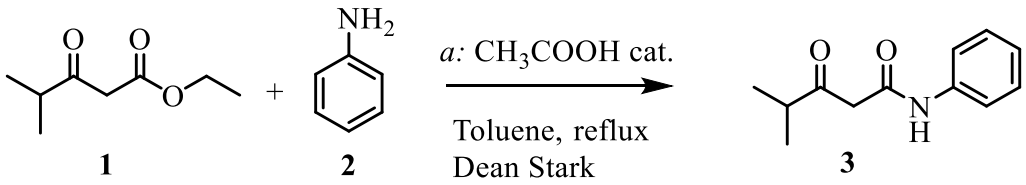

A solution of ethyl 4-methyl-3-oxopentanoate **2** (5g; 0.0316mmol; 1eq.), aniline **1** (2.89 mL, 0.0319 mmol, 1 eq), and acetic acid (0.063 mL) in toluene (38 mL) was refluxed for 4 h with a Dean-Stark apparatus. The cold mixture was washed twice with a solution of hydrochloric acid 2 M (5 mL), twice with a saturated solution of sodium bicarbonate (10 mL), extracted with EtOAc (30 mL x 3) and washed with a solution of brine (15 mL x 2). The product **3** was obtained as a pale yellow oil with a yield of 42% (2.74 g), and crystallized with hot hexane to give a white crystal.

*4-methyl-3-(methylamino)-N-phenylpent-2-enamide [**4**]*

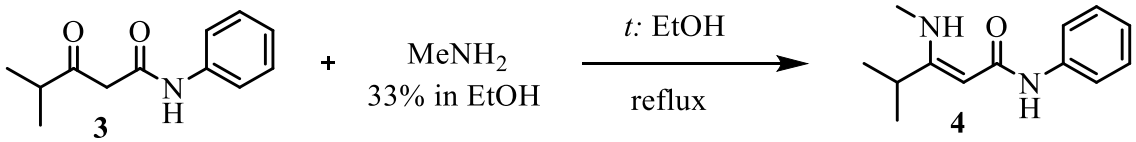

To a solution of 4-methyl-3-oxo-*N*-phenylpentanamide **3** (3.72 g, 14.98 mmol), in ethanol (0.5 M, 7.49 mL) was added methylamine (33%^{w} solution in ethanol, 17.27 mL) and the resulting solution was refluxed for 7 h and concentrated in vacuo.

4) 4-methyl-3-(methylamino)-N-phenylhex-2-enamide

^{1}H NMR (600 MHz, CD_3CN, 1.96 ppm, 25 °C) δ 1.14 (d, J = 6.97p, 6H), 2.77 (sept. J = 6.97 Hz, 1H), 2.92 (d, J = 5.35 Hz, 3H), 4.60 (s, 1H), 6.96 (t, J = 7.39 Hz, 1H), 7.24 – 7.28 (m, 2H), 7.52 (d, J = 8.54 Hz, 2H), 6.67 (s broad, 1H), 9.21 (s broad, 1H); **^{13}C NMR** (150.8 MHz, CD_3CN, s 118.26 ppm, 25 °C) δ 21.6 (2 CH_3), 28.9 (CH), 29.1 (CH_3), 81.2 (CH), 119.6 (2 CH), 122.8 (CH), 129.6 (2 CH), 141.5 (Cq), 170.8 (Cq), 171.7 (Cq).

*Compound β-nitrostyrene [**6a-c**]*

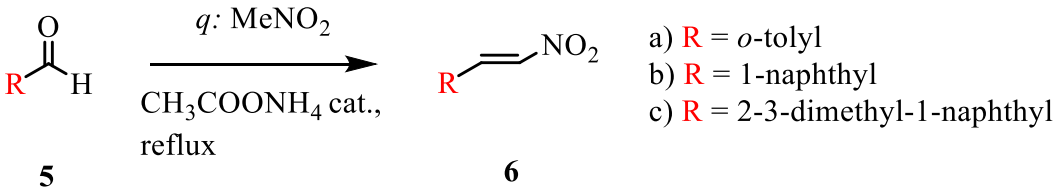

5 **6**

A stirred mixture of the aldehyde (3 mmol, 1 eq), ammonium acetate (69.4 mg, 0.9 mmol, 0.3eq.) and nitromethane (8.83 mL, 165 mmol, 55 eq) was refluxed for 1.5-2 h (monitored by TLC, petroleum ether/dichloromethane 7:3). After this period, the mixture was treated with a saturated aqueous solution of $NaHCO_3$ (30 mL) and extracted with CH_2Cl_2 (30 mL x 3). The combined organic phases were dried over anhydrous Na_2SO_4 and the nitromethane was distilled under reduced pressure. The mixture obtained with a yield of 98% was used for the next procedure.

6a) (E)-1-methyl-2-(2-nitrovinyl)benzene

^{1}H NMR (600 MHz, $CDCl_3$, TMS, 25 °C) δ 2.48 (s, 3H), 7.23-7.29 (m, 2H), 7.38 (t, J = 7.67 Hz, 1H), 7.49-7.52 (m, 2H), 8.29 (d, J = 13.62 Hz, 1H); **^{13}C NMR** (150.8 MHz, $CDCl_3$ 77.16 ppm, TMS, 25 °C) δ 17.1(CH_3), 123.93(CH), 124.5 (CH), 126.1 (Cq), 128.5 (CH), 129.1 (CH), 133.9 (CH), 134.8 (CH), 136.4 (Cq)

6b) (E)-1-(2-nitrovinyl)naphthalene

^{1}H NMR (600 MHz, CD_3CN, 1.96 ppm, 25 °C) δ 7.56 (t, J = 7.74 Hz, 1H), 7.60-7.68 (m, 2H), 7.82(d, J = 13.35 Hz, 1H), 7.89 (d, J = 7.34 Hz, 1H), 7.98 (d, J = 8.00 Hz, 1H), 8.07 (d, J = 8.34 Hz, 1H), 8.20 (d, J = 8.51 Hz, 1H), 8.82 (d, J = 13.35 Hz, 1H); **^{13}C NMR** (150.8 MHz, CD_3CN, s 118.26 ppm, 25 °C) δ 124.1 (CH), 126.5 (CH), 127.6_7 (CH), 127.7_3 (CH), 128.1 (Cq), 128.5 (CH), 129.9 (CH), 132.3 (Cq), 133.2 (CH), 134.7 (Cq), 136.6 (CH), 140.0 (CH).

6c) (E)-2,3-dimethyl-1-(2-nitrovinyl)naphthalene

^{1}H NMR (600 MHz, CD_3CN, 1.96 ppm, 25 °C) δ 2.15 (s, 3H), 2.20 (s, 3H), 7.13 (d, J = 13.91, 1H), 7.21-7.25 (m, 2H), 7.47 (s, 1H), 7.53-7.56 (m, 1H), 7.65-7.68 (m, 1H), 8.23 (d, J = 13.91 Hz, 1H); **^{13}C NMR** (150.8 MHz, CD_3CN, s 118.26 ppm, 25 °C) δ 17.7 (CH_3), 21.0 (CH_3), 125.1 (CH), 126.6 (CH), 126.9 (Cq), 127.1 (CH), 128.6 (CH), 130.6 (CH), 131.0 (Cq), 133.0 (Cq), 136.5 (Cq), 136.7 (Cq), 137.8 (CH), 143.5 (CH).

Compound β-bromonitroalkene [7a-f]

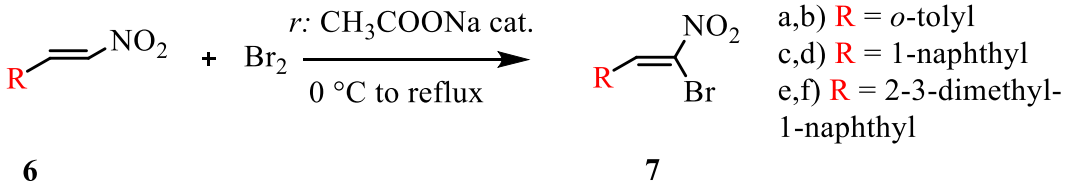

6 **7**

To a stirred solution of β-nitrostyrene (2.94 mmol, 1eq) in sodium acetate (289.58 mg, 3.53 mmol, 1.2 eq) and chloroform (1 M), Br_2 (0.18 mL, 3.53 mmol, 1.2 eq) was added dropwise over 5 min at 0 °C. The cloudy yellow reaction was then heated to reflux and stirred for 6-8 h (monitored by TLC hexane/dichloromethane (6:4). The excess of Br_2 was removed by washing with a saturated aqueous solution of $Na_2S_2O_3$ (10 mL). The solution was extracted with CH_2Cl_2 (10 mL x 3). The combined organic layers were dried over anhydrous Na_2SO_4. The solvent was removed by evaporated under reduce pressure to give a crude solid that was purified by flash silica chromatography using hexane/dichloromethane (7:3).

7a+b) (E+Z)-1-(2-bromo-2-nitrovinyl)-2-methylbenzene (23:77)

Yield : Z = 58.72%; E = 1.19%

Analyzed in mixture

^{1}H NMR (400 MHz, CD_3CN, 1.96 ppm, 25 °C) δ 2.32 (s, 3H, isom. E), 2.37 (s, 3H, isom. Z), 7.13 – 7.24 (m, 2H, isom. E), 7.30 – 7.34 (m, 1H, isom. E), 7.34 – 7.37 (m, 2H isom. Z), 7.40 – 7.42 (m, 1H, isom.Z), , 7.42 – 7.45 (m, 1H, isom. E), 7.53 (s, 1H, isom. E), 7.72 (d, J= 8.06 Hz, 1H, isom. Z), 8.76 (s, 1H, isom. Z) ; **^{13}C NMR** (100 MHz, CD_3CN, s 118.26 ppm, 25 °C) δ 19.9 (CH_3, isom. E), 20.0 (CH_3, isom. Z), 126.9 (CH, isom. Z), 127.2 (CH, isom. E), 128.0 (CH, isom. E), 129.4 (CH, isom. Z), 130.6 (CH, isom. E), 131.2 (CH, isom. E), 131.3_8 (Cq, isom. E), 131.4 (CH, isom. Z), 131.6 (Cq, isom. Z), 131.8 (CH, isom. Z), 133.1 (Cq, isom. E), 135.1 (CH, isom. E), 137.3 (Cq, isom. Z), 137.3_2 (CH, isom. Z), 139.5 (Cq, isom. Z).

7c) (E)-1-(2-bromo-2-nitrovinyl)naphthalene

Yield = 3.10%

^{1}H NMR (600 MHz, $CDCl_3$, TMS, 25 °C) δ 7.40 – 7.47 (m, 2H), 7.54 – 7.61 (m, 2H), 7.68 (s, 1H), 7.86 (d, J = 8.42 Hz, 1H), 7.88 – 7.91 (m, 2H); **^{13}C NMR** (150.8 MHz, $CDCl_3$ 77.16 ppm, TMS, 25 °C) δ 123.9 (CH), 125.6 (CH), 126.2 (CH), 126.8 (CH), 127.4 (CH), 129.0 (CH), 129.5 (Cq), 130.5 (CH), 130.5_3 (Cq), 132.1 (CH), 133.6 (Cq).

7d) (Z)-1-(2-bromo-2-nitrovinyl)naphthalene

Yield = 28.08%

^{1}H NMR (600 MHz, $CDCl_3$, TMS, 25 °C) δ 7.55 – 7.65 (m, 3H), 7.90 – 8.02 (m, 4H), 9.20 (s, 1H); **^{13}C NMR** (150.8 MHz, $CDCl_3$ 77.16 ppm, TMS, 25 °C) δ 123.6 (CH), 125.2 (CH), 127.0 (CH), 127.7 (CH), 128.0 (CH), 128.1 (Cq), 129.2 (CH), 131.3 (Cq), 131.5 (Cq), 131.8 (CH), 133.6 (Cq), 135.1 (CH).

7e) (E)-1-(2-bromo-2-nitrovinyl)-2,3-dimethylnaphthalene

Yield = 3.12%

^{1}H NMR (600 MHz, CD_3CN, 1.96 ppm, 25 °C) δ 2.34 (s, 3H), 2.48 (s, 3H), 7.44 – 7.52 (m, 2H), 7.69 (d, J = 8.27 Hz, 1H), 7.77 (s, 1H), 7.83 (d, J = 8.03 Hz, 1H), 8.99 (s, 1H); **^{13}C NMR** (150.8 MHz, CD_3CN, s 118.26 ppm, 25 °C) δ 17.5 (CH_3), 20.7 (CH_3), 125.2 (CH), 126.7 (CH), 127.0 (CH), 128.6 (CH), 128.7 (Cq), 129.4 (Cq), 130.0 (CH), 133.0 (Cq), 134.8 (Cq), 134.9 (Cq), 136.8 (Cq), 139.3 (CH).

7f) (Z)-1-(2-bromo-2-nitrovinyl)-2,3-dimethylnaphthalene

Yield = 22.06 %

^{1}H NMR (600 MHz, CD_3CN, 1.96 ppm, 25 °C) δ 2.37 (s, 3H), 2.50 (s 3H), 7.46 – 7.53 (m, 2H), 7.71 (d, J = 8.33 Hz, 1H), 7.80 (s, 1H), 7.85 (d, J = 8.03 Hz, 1H), 9.04 (s, 1H); **^{13}C NMR** (150.8 MHz, CD_3CN, s 118.26 ppm, 25 °C) δ 17.5 (CH_3), 20.7 (CH_3), 125.2 (CH), 126.7 (CH), 126.9 (CH), 128.6 (CH), 128.7 (Cq), 129.3 (Cq), 130.0 (CH), 133.0 (Cq), 134.8 (Cq), 134.9 (Cq), 136.8 (Cq), 139.3 (CH).

Compound hindered phenyl-nytroalkene [9a-f]

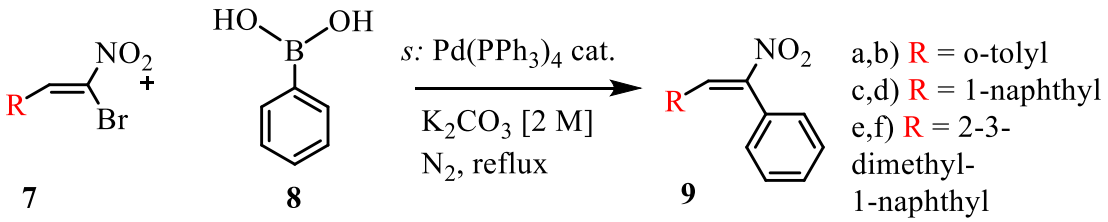

To a solution of compound β-bromonitroalkene (1 mmol, 1eq) in toluene/CPME (19:1, 3.28 mL) was added the phenylboronic acid (0.183 g, 1.5 mmol, 1,5 eq) and a solution of K_2CO_3 (2 M, 1.20 mL) the mixture was degassed with cycles of vacuum/nitrogen. Over nitrogen flow, was added a catalytic amount of $Pd(PPh_3)_4$ and refluxed for 3 to 12 hours based on the colour change of the mixture. The solution was then concentrated in vacuo, and the product was extracted with EtOAc/water. The combined organic layer was dried over Na_2SO_4 concentrated in vacuum, and the product was purified by column chromatography with petroleum ether and dichloromethane 60:40

9a) (E)-1-methyl-2-(2-nitro-2-phenylvinyl)benzene

Yield = 56.41%

^{1}H NMR (600 MHz, $CDCl_3$, TMS, 25 °C) δ 2.45 (s, 3H), 6.75 (d, J = 7.87 Hz, 1H), 6.89 (t, J = 7.48 Hz, 1H), 7.15 – 7.22 (m, 2H), 7.24 – 7.28 (m, 2H), 7.36 – 7.45 (m, 3H), 8.38 (s, 1H)); **^{13}C NMR** (150.8 MHz, $CDCl_3$ 77.16 ppm, TMS, 25 °C) δ 20.4(CH_3), 126.0 (CH), 129.0 (2 CH), 129.6 (Cq), 129.8 (CH), 130.1 (CH), 130.2 (CH), 130.6 (Cq), 130.7 (2 CH), 132.8 (CH), 138.8 (Cq), 150.6 (broad Cq).

9b) (Z)-1-methyl-2-(2-nitro-2-phenylvinyl)benzene

Yield = 15.02%

^{1}H NMR (600 MHz, CD_3CN, 1.96 ppm, 25 °C) δ 2.38 (s, 3H), 7.21 – 7.29 (m, 3H), 7.30 – 7.35 (m, 2H), 7.51- 7.57 (m, 5H); **^{13}C NMR** (150.8 MHz, CD_3CN, s 118.26 ppm, 25 °C) δ 20.0 (CH_3), 123.7 (CH), 126.9 (2 CH), 127.2 (CH), 127.8 (CH), 130.2 (CH), 130.3 (CH), 131.1_6 (CH), 131.1_7 (CH), 132.0 (Cq), 132.9 (Cq), 138.2 (Cq), 153.3 (broad Cq).

9c) (E)-1-(2-nitro-2-phenylvinyl)naphthalene

Yield = 32.13%

^{1}H NMR (600 MHz, CD_3CN, 1.96 ppm, 25 °C) δ 7.14 (d, J = 7.14 Hz, 1H), 7.23 – 7.44 (m, 6H), 7.58 – 7.69 (m, 2H), 7.88 (d, J = 7.99 Hz, 1H), 7.94 (d, J = 8.19 Hz, 1H), 8.16 (d, J = 8.38 Hz, 1H), 8.85 (s, 1H); **^{13}C NMR** (150.8 MHz, CD_3CN, s 118.26 ppm, 25 °C) δ 125.1 (CH), 126.0 (CH), 127.6 (CH), 128.1 (CH), 129.1 (CH), 129.4 (2 CH), 129.6 (CH), 130.2 (Cq), 130.6 (CH), 131.1 (CH), 131.5 (Cq), 131.7 (2 CH), 132.5 (Cq), 134.0 (CH), 134.3 (Cq), 153.1 (broad Cq)

9d) (Z)-1-(2-nitro-2-phenylvinyl)naphthalene

Yield = 17.21%

^{1}H NMR (600 MHz, CD_3CN, 1.96 ppm, 25 °C) δ 7.50 – 7.55 (m, 2H), 7.55 – 7.59 (m, 3H), 7.60 – 7.65 (m, 4H), 7.75 (broad, 1H), 7.97 – 8.01 (m, 2H), 8.06 – 8.09 (m, 1H); **^{13}C NMR** (150.8 MHz, CD_3CN, s 118.26 ppm, 25 °C) δ 123.0 (CH), 125.3 (CH), 126.4 (CH), 126.6 (CH), 127.1 (2 CH), 127.7 (CH), 128.0 (CH), 129.6 (CH), 130.2 (2 CH), 130.6 (CH), 131.1 (Cq), 131.4 (CH), 132.0 (Cq), 131.1 (Cq), 134.4 (Cq), 154.6 (broad Cq).

9e) (E)-2,3-dimethyl-1-(2-nitro-2-phenylvinyl)naphthalene

Yield = 9.62%

^{1}H NMR (600 MHz, CD_3CN, 1.96 ppm, 25 °C) δ 2.27 (s, 3H), 2.36 (s, 3H), 7.13 – 7.17 (m, 4H), 7.19 – 7.24 (m, 1H), 7.38 – 7.42 (m, 2H), 7.62 (s, 1H), 7.70 -7.73 (m, 1H), 7.82 – 7.86 (m, 1H), 8.56 (s, 1H); **^{13}C NMR** (150.8 MHz, CD_3CN, s 118.26 ppm, 25 °C) δ 17.7 (CH_3), 20.7 (CH_3), 125.6 (CH), 126.5 (CH), 126.6 (CH), 128.4 (CH), 128.7 (Cq), 128.9 (2CH), 129.4 (CH), 130.2 (Cq), 130.5 (CH), 130.8 (2CH), 131.1 (Cq), 132.8 (Cq), 134.8 (Cq), 135.1 (CH), 136.5 (Cq), 154.2 (Cq).

9f) (Z)-2,3-dimethyl-1-(2-nitro-2-phenylvinyl)naphthalene

Yield = 3.25%

^{1}H NMR (600 MHz, CD_3CN, 1.96 ppm, 25 °C) δ 2.41 (s, 3H), 2.47 (s, 3H), 7.42 -7.48 (m, 2H), 7.54 – 7.48 (m, 4H), 7.63 – 7.67 (m, 2H), 7.71 (s, 1H), 7.78 – 7.85 (m, 2H)); **^{13}C NMR** (150.8 MHz, CD_3CN, s 118.26 ppm, 25 °C) δ 17.7(CH_3), 20.8 (CH_3), 125.2 (CH), 125.6 (CH), 126.5 (CH), 126.6 (CH), 127.5 (2CH), 128.4 (CH), 129.1 (Cq), 129.2 (CH), 130.1 (2CH), 130.8 (Cq), 131.4 (CH), 131.8 (Cq), 133.0 (Cq), 135.2 (Cq), 136.6 (Cq), 155.3 (Cq).

Hindered pyrrole compound 10a-b

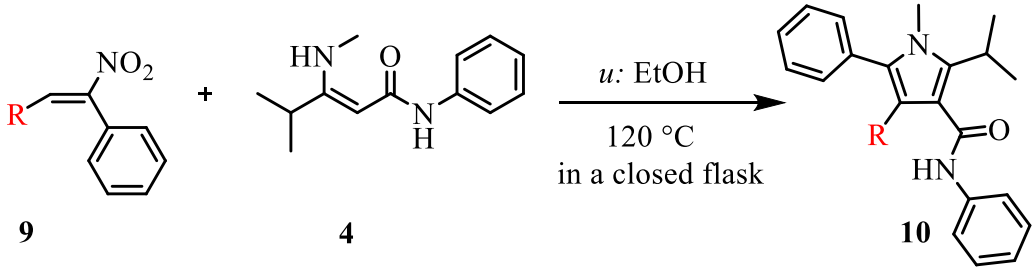

9 **4** **10**

a) R = o-tolyl
b) R = 1-naphthyl

To a solution of hindered alkene (0.1 mmol, 1 eq), in ethanol (0.1 M), was added compound **4** (21.8 mg, 0.1 mmol, 1 eq). The solution was heated to +120 °C in a closed flask for 8h, the resulting yellow pale solution was treated over chromatography column with petroleum ether and dichloromethane (1:1).

10a) 2-isopropyl-1-methyl-N,5-diphenyl-4-(o-tolyl)-1H-pyrrole-3-carboxamide

Yield = 6.40%

^{1}H NMR (600 MHz, $C_2D_2Cl_2$, 6 ppm, 25 °C) δ 1.50 (d, J = 7.22 Hz, 3H), 1.51 (d, J = 7.2 Hz, 3H), 2.07 (s, 3H), 3.57 (s, 3H), 4.25 (sept, J = 7.2 Hz, 1H), 6.94 – 6.99 (m, 3H), 7.01 (s, 1H), 7.11 – 7.30 (m, 11H); **^{13}C NMR** (600 MHz, $C_2D_2Cl_2$, 73.78 ppm, 25 °C) δ 20.1 (CH_3), 20.7 (CH_3), 20.8 (CH_3), 25.2 (CH), 33.4 (CH_3), 74.16 (CH_3) 113.5 (Cq), 119.2 (2 CH), 119.4 (Cq), 123.0 (CH), 126.0 (CH), 127.1 (CH), 127.7 (CH), 127.9 (2 CH), 128.6 (2 CH), 130.2 (CH), 130.6 (2 CH), 130.9 (Cq), 131.7 (Cq), 131.9 (CH), 134.8 (Cq), 138.5 (Cq), 138.6 (Cq), 143.5 (Cq), 164.0 (Cq).

10b) 2-isopropyl-1-methyl-4-(naphthalen-1-yl)-N,5-diphenyl-1H-pyrrole-3-carboxamide

Yield = 41.95%

^{1}H NMR (600 MHz, CD_3CN, 1.96 ppm , 25 °C) δ 1.50 (d, J = 7.1 Hz, 3H), 1.51 (d, J = 7.1 Hz, 3H), 3.58 (s, 3H), 3.80 (sept, J = 7.1 Hz, 1H), 6.75 – 6.78 (m, 2H), 6.86 (t, J = 7.4 Hz, 1H), 7.00 – 7.06 (m, 2H), 7.13 – 7.21 (m, 5H,), 7.25 (s, 1H), 7.38 – 7.46 (m, 4H), 7.78 - 7.87 (m, 3H); **^{13}C NMR** (150.8 MHz, CD_3CN, s 118.26 ppm, 25 °C) δ 21.1 (CH_3), 21.5 (CH_3), 26.8 (CH), 33.4 (CH_3), 117.5 (Cq), 119.1 (Cq), 119.7 (2 CH), 124.1 (CH), 126.3 (CH), 126.9 (CH), 127.0 (CH), 127.3 (CH), 128.5 (CH), 128.6 (CH), 128.9 (2 CH), 129.1 (CH), 129.4 (2 CH), 130.4 (CH), 131.6 (2 CH), 132.6 (Cq), 133.0 (Cq), 134.5 (Cq), 134.4_7 (Cq), 134.5_2 (Cq), 139.6 (Cq), 142.2 (Cq), 165.4 (Cq).

Platform pyrrole

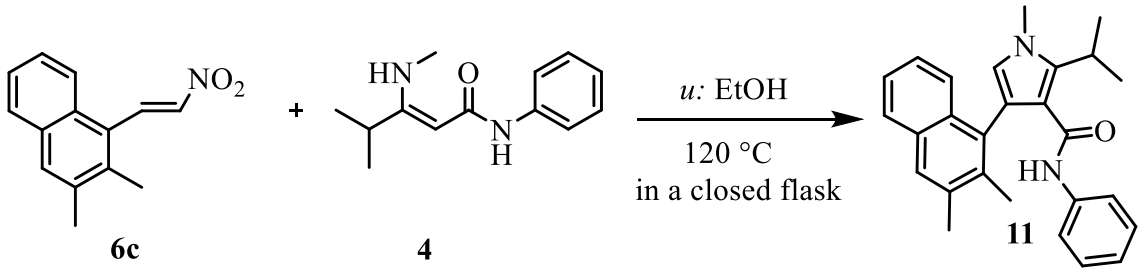

6c **4** **11**

To avoid the problem due the steric hindered in the closure of the pyrrole compound, we decide to make the same reaction with compound **6c** for obtaining the pyrrole and after proceed with the bromination and the Suzuki reaction, the result is the same hindered compound.

To a solution of alkene **6c** (179.4 mg, 0.79 mmol, 1eq), in ethanol (7.90 mL, 0.1 M), was added compound **4** (172.3 mg, 0.79 mmol, 1 eq). The solution was heated to 120 °C in a closed flask for 8h, the resulting yellow pale solution was treated over chromatography column with petroleum ether and dichloromethane (1:1).

11) 4-(2,3-dimethylnaphthalen-1-yl)-2-isopropyl-1-methyl-N-phenyl-1H-pyrrole-3-carboxamide

Yield = 29.24%

^{1}H NMR (600 MHz, CD_3CN, 1.96 ppm , 25 °C) δ 1.48 (d, J = 7.3 Hz, 3H), 1.49 (d, J = 7.3 Hz, 3H), 2.29 (s, 3H), 2.51 (s, 3H), 3.78 (s, 3H), 3.99 (sept, J = 7.3 Hz, 1H), 6.51 (s, 1H), 6.64 – 6.70 (m, 2H), 6.83 – 6.90 (m,1H), 7.00 – 7.11 (m broad, 3H), 7.33 – 7.46 (m, 2H), 7.61 (d, J = 8.3 Hz, 1H), 7.79 (s, 1H), 7.83 (d, J = 8.3 Hz, 1H); **^{13}C NMR** (150.8 MHz, CD_3CN, s 118.26 ppm, 25 °C) δ 20.0 (CH_3), 20.9 (CH_3), 23.0 (CH_3), 21.2 (CH_3), 26.3 (CH), 35.9 (CH_3), 116.0 (Cq), 119.1 (CH), 119.3 (Cq), 122.6 (CH), 123.8 (CH), 126.3 (CH), 126.5 (CH), 126.8 (CH), 128.1 (CH), 128.6 (CH), 129.5 (CH), 132.2 (Cq), 133.2 (Cq), 133.7 (Cq), 136.9 (Cq), 137.2 (Cq), 139.7 (Cq), 144.0 (Cq), 164.8 (Cq).

Bromurated pyrrole

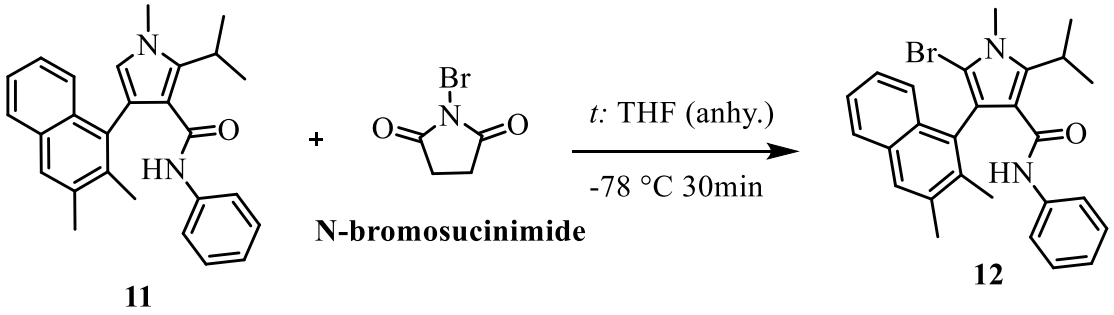

11 **N-bromosucinimide** **12**

The pyrrole **11** (85.29 mg, 0.23 mmol, 1eq) was dissolved in dry THF (2.30 mL, 0.1 M) and cooled to -78 °C. *N*-bromosuccinimide (44.76 mg, 0.25_3 mmol, 1.1 eq), was added and the temperature was maintained for 30 min., after the reaction was allowed to cool to room temperature and was stirred for and additional hour. After purification via silica gel (hexane/dichloromethane 8:2) the product obtained was a white solid (60.78 mg, 0.13 mmol, Yield = 55.74%).

12) 5-bromo-4-(2,3-dimethylnaphthalen-1-yl)-2-isopropyl-1-methyl-N-phenyl-1H-pyrrole-3-carboxamide

^{1}H NMR (600 MHz, CD_3CN, 1.96 ppm , 25 °C) δ 1.47 (d, J = 7.7 Hz, 3H), 1.48 (d, J = 7.7 Hz, 3H), 2.26 (s, 3H), 2.51 (s, 3H), 3.78 (s, 3H), 4.00 (sept, J = 7.70 Hz, 1H), 6.67 – 6.73 (m, 2H), 6.88 (t, J = 7.5 Hz, 1H), 7.05 (m, 2H), 7.14 (broad s, 1H), 7.37 – 7.51 (m, 3H), 7.82 (s, 1H), 7.85 (d, J = 8.1 Hz, 1H); **^{13}C NMR** (150.8 MHz, CD_3CN, s 118.26 ppm, 25 °C) δ 17.6 (CH_3), 20.9 (CH_3), 21.0 (CH_3), 21.2 (CH_3), 27.1 (CH), 34.6 (CH_3), 104.6 (Cq), 117.0 (Cq), 119.5 (2 CH), 119.7 (Cq), 124.2 (CH), 126.2 (CH), 126.5 (CH), 126.9 (CH), 128.4 (CH), 129.2 (CH), 129.5 (2 CH), 131.1 (Cq), 132.9 (Cq), 133.3 (Cq), 137.0 (Cq), 137.6 (Cq), 139.4 (Cq), 144.7 (Cq), 164.1 (Cq).

Hindered pyrrole

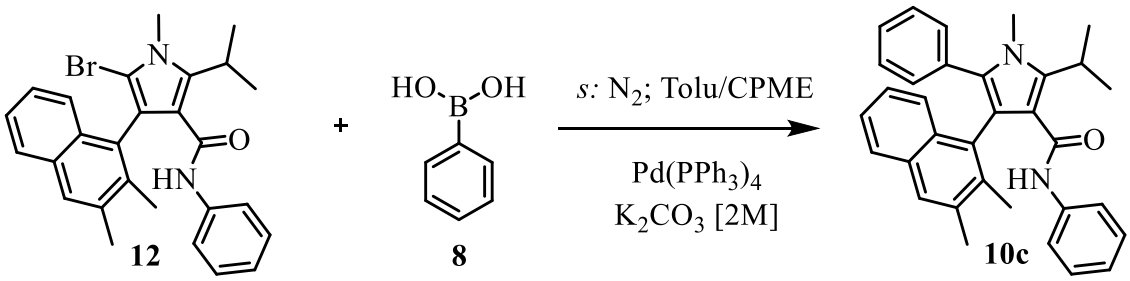

To a solution of compound **12** (24.5 mg, 0.052 mmol, 1eq) in toluene/CPME (19:1, 0.17 mL) was added the phenylboronic acid (9.51 mg, 0.078 mmol, 1,5 eq) and a solution of K_2CO_3 (2 M, 62.4 µL) the mixture was degassed with cycles of vacuum/nitrogen. Over nitrogen flow, was added a catalytic amount of $Pd(PPh_3)_4$ and refluxed for 3 h. The solution was then concentrated in vacuum, and the product was extracted with EtOAc/water. The combined organic layer was dried over Na_2SO_4 concentrated in vacuum, and the product was purified by column chromatography with petroleum ether and dichloromethane 50:50.

The product was a white solid (18.75 mg, 0.040 mmol, Yield = 76.92%)

10c) 4-(2,3-dimethylnaphthalen-1-yl)-2-isopropyl-1-methyl-N,5-diphenyl-1H-pyrrole-3-carboxamide

^{1}H NMR (600 MHz, CD_3CN, 1.96 ppm , 25 °C) δ 1.53 (d, J = 7.3 Hz, 3H), 1.54 (d, J = 7.3 Hz, 3H), 2.22 (s, 3H), 2.40 (s, 3H), 3.60 (s, 3H), 4.03 (sept, J = 7.3 Hz, 1H), 6.65 – 6.68 (m, 2H), 6.86 (t, J = 7.5 Hz, 1H), 7.00 – 7.20 (m, 8H), 7.35 – 7.43 (m, 2H), 7.63 – 7.60 (m 2H), 7.76 (d, J = 7.7 Hz, 1H); **^{13}C NMR** (150.8 MHz, CD_3CN, s 118.26 ppm, 25 °C) δ 18.0 (CH_3), 21.0 (CH_3), 21.1_0 (CH_3), 21.1_4 (CH_3), 26.7 (CH), 33.7 (CH_3), 115.8 (Cq), 117.8 (Cq), 119.4 (2 CH), 123.9 (CH), 126.3 (CH), 126.7 (CH), 126.8 (CH), 128.3 (CH), 128.5 (CH), 128.6 (CH), 128.9 (2 CH), 129.5 (2 CH), 131.0 (2 CH), 133.3 (Cq), 132.4 (Cq), 133.1 (Cq), 133.3 (Cq), 133.7 (Cq), 136.8 (Cq), 137.5 (Cq), 139.7 (Cq), 144.1 (Cq), 165.0 (Cq).

6. Appendix

6.1. Defining the energy barriers

Individuated the substituent that could develop the searching rotational energy, this energy gets defined with computational methods. The base of the calculation is to find the most stable conformation, individuated by the geometry that minimizes the repulsion energy and therefore shows the lowest potential energy.

Geometry analysis is the study that is refined by different computation methods, in the early stage of studies a Molecular Mechanics (MM) model is used for defining the starting geometry and then a DFT method is used to find the energy with more accuracy.

The MM method was the first kind of computational methods largely available thanks to short computational methods with quite accurate results. The MM computation uses the classical mechanics to model molecular system considered as a collection of "beads" (atom-like particles) connected by springs (bonds), the potential energy of the molecule is then calculated as a function of the nuclear coordinates using force field (FF), assumed the *Born-Oppenheimer approximation*[a].

The FF is an arbitrary list of coefficients that represent all chemical information, defining all the functionals and parameters sets that represent the MM computation, it could be fitted in accordance with the class of molecules (alkanes, amino acids, etc.) to reproduce a range of thermodynamic and structural properties. [36-37]

MM is a rough system for our studies, because even if the energies of the ground state (with some limitations) are pretty precise, the energies far from the global minimum are very poorly accurate, usually the geometry of the transition state needs to be manually built and the energy is calculated by moving the relative part of the molecule in fixed steps and optimizing the remaining part. Even if the transition state was found, there was no indication regarding the presence of a more stable geometry, this kind of computational analysis proceeds with a trial and error approach. This is a huge limitation for the prediction of the rotational energy barriers, so, found the rough geometry of the

[a] Is the assumption that the motion of atomic nuclei and electrons can be separated, useful in mathematical terms because allows the wavefunction of a molecule to be broken into its electronic and nuclear components

molecule we adopt other methods for defining the minimum potential energy and the transition state. [38]

To obtain an highly accurate computation of the energy barriers, we used the software Gaussian09 that allows us a high-level of calculations in a reasonable amount of time, for molecules containing up to 50-100 atoms.

This kind of software is based on the Hartree-Fock (HF) and density functional theory (DFT) methods to evaluate the energy of molecules.

The HF is a method of approximation, to determine the energy of a quantistic many-body system in a stationary state (or can determinate the relative wave function), assuming that the wave-function on the n-body could be approximated by a single *Slatter determinant*[b].[39] Using this approximation it is possible to find the energy of the ground state of a molecule by solving the Schrödinger equation minimizing the total-energy wave-function functionals allowing only the Slatter determinant to be a variable function.[40] This is a self-consistent method that can compute the final field from the charge distribution of the starting configuration but neglecting the electronic correlation is a serious limitation.

The DFT uses the hypothesis that the electron density (ρ) is the key step to define the proprieties of a many-body system, determining the proprieties of many-electron system using functionals.

The essential theory of the DFT is the following: for a collection of electrons and nuclei the ground state molecular energy, the wavefunction and all other molecular electronic properties are uniquely determined by the $\rho(x,y,z)$, a function of three variables, in which the ground state energy, E_0, is a functional of the density ρ: $E_0 = F[\rho]$.

This theory demonstrates that an accurate combination of appropriate functionals with the electron density can define the molecular energy, with the great advantage of considering the electronic correlation, improving performance and accuracy with respect of computational methods, at a reasonable computational cost.[41]

[b] It is an expression that describes the wave function of a multi-femionic system that satisfies anti-symmetry requirements and consequently the Pauli principle, by changing sign upon the exchange of two electrons.

The value of the software is the possibility to use a hybrid or pure functional to determine the potential energy. In our study we used the hybrid functional Becke-3-LYP that combines linearly the exchange energy (defined in the Hartree-Fock methods) and the exchange-correlation functional (defined by the density function theory) to evaluate the ground states and the transition state.

The potential energy associated to a non-excited geometry at 25 °C is defined ground state (GS), for accuracy consideration the smallest basis set used is generally 6-31G* or the equivalent. Interestingly, there is only a small increase in accuracy obtained by using very large basis sets. This is probably due to the fact that the density functional has limited accuracy compared to that of the basis set. The accuracy of results from DFT calculations can be poor to fairly good, depending on the choice of basis set and density functional.

The geometries obtained by calculations can in many cases be checked by X-ray diffraction data, and the relative energies of conformations can be compared with the results of variable- temperature NMR spectroscopy. Although such a calculation usually refers to an isolated molecule, whereas X-ray studies reflect the solid state and NMR results are for solutions, DFT structures compare experimental observations very well in almost all cases, and the relative energies of possible conformations are correctly calculated.

Different geometries are possible depending on the arrangement of the different groups, that allows to individuate different minima of energy for one molecule, which can differ from each other of several kcal/mol, so the different GS was selected taking as a reference the lowest gained energy. This process is necessary for the calculation of the *Boltzmann population* at 25 °C, knowing this, we consider the structures populated when they have a $\Delta E \leq 1$ kcal/mol.

The determination of transition state (TS) structures and energies is a crucial point for dynamic analysis, because the correct simulation of energy barriers could greatly help the understanding of dynamic processes. As addressed by D. Young,[42] a transition state (or saddle point) structure is mathematically defined as "*the geometry that has zero derivative of energy with respect to moving every one of the nuclei, and has positive second derivative energy for all but one geometric movement*". In other words, a transition state linking two energy minima represents a maximum of energy in the direction of the reaction path, but it is a minimum in all other directions. [Figure 46]

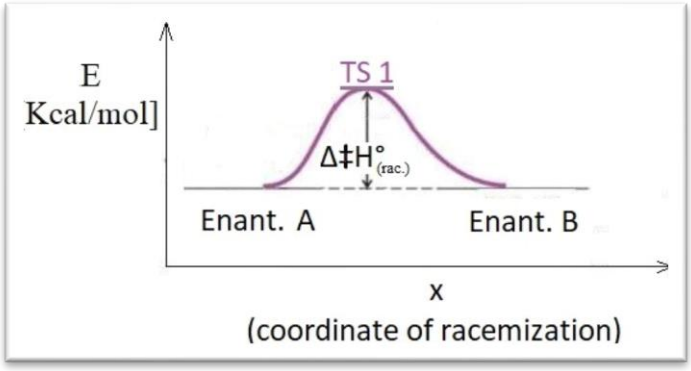

Figure 46: 2D simplified graph of a racemization process, Enant.A and Enant.B are mirror configuration of one GS. $\Delta^{\ddagger}H°$ and $\Delta G^{\ddagger}$ represent the same energy in the case where $\Delta S^{\ddagger} = 0$. During the racemization process, the variation of entropy it is often overlooked.

Once a stationary point is found, the primary way to verify whether it corresponds to a transition state is to compute the vibrational frequencies. A transition state must have only one negative (i.e., imaginary) frequency, and the vibrational motion associated with this frequency corresponds to the motion going towards the reagent in one direction and towards the product in the other direction.

Unfortunately, in contrast with the transition states for high-energy processes (such as those involved in a chemical reaction), in which the imaginary frequency usually has a large (negative) value, the transition states involved in internal dynamic processes usually display small negative vibrational frequencies and therefore it can be difficult to locate, especially in the presence of other possible internal motions. On the other hand, the geometry of a transition state is much simpler to idealise, because many geometrical parameters are fixed by the molecular scaffold.

The predicted rotational energy is the minor difference from the lowest GS and the lowest TS.

6.2. Stereochemistry analysis

Computational calculation can provide a prediction of the behaviour of the molecules but this must be verified by the experimental tests. In order to define the conformational stability of organic molecules, methods have been established to determine the dynamic stereochemical proprieties.

Dynamic Nuclear Magnetic Resonance (D-NMR) and dynamic High Performance Liquid Chromatography (D-HPLC) are considered to be the most useful experimental methods.

NMR can observe the conformational exchange of chemical species that happens at a rate sufficiently low to observe separate anisochronous signals, in the milliseconds-seconds region:

$$t = \frac{\sqrt{2}}{2\pi\,\Delta\nu} \qquad 1.2$$

Where:

t = conformational exchange time(s);

Δv = chemical shift difference (in Hz) without exchange.

Through this equation it can be affirmed that two exchanging nuclei can display different chemical shifts (Δv) when they occupy two positions with a different magnetic environment for a time longer than the conformational exchange time (t).

Analysing the spectrum of an atropisomeric compound, two enantiomers can be distinguished from the chemical shift of the signals called *chirality probes*.

These chirality probes are diastereotopic groups that display different chemical shifts when they are placed in a chiral environment. In the atorvastatin molecule, the probe is defined by the *i*-Pr group already present in the initial molecule.

To compare the acquisition time of the NMR with the kinetic processes, the spectra are acquired at different temperatures as an indication of conformational processes that occur in the time scale of NMR, enabling to observe the overlap or resolution of the signals relatives to the chirality probes.

When the rotation around a chirality axis is obstructed and results slow in NMR scale, each diastereotopic group experiences a magnetically different environment for a time

long enough to be detected, resulting two different signals. Once the temperature is raised, the process occurs faster and the signals broaden until the coalescence point is reached. At this temperature, the two enantiomers are no longer distinguishable and only one broad peak is observable.[43] [Figure 47]

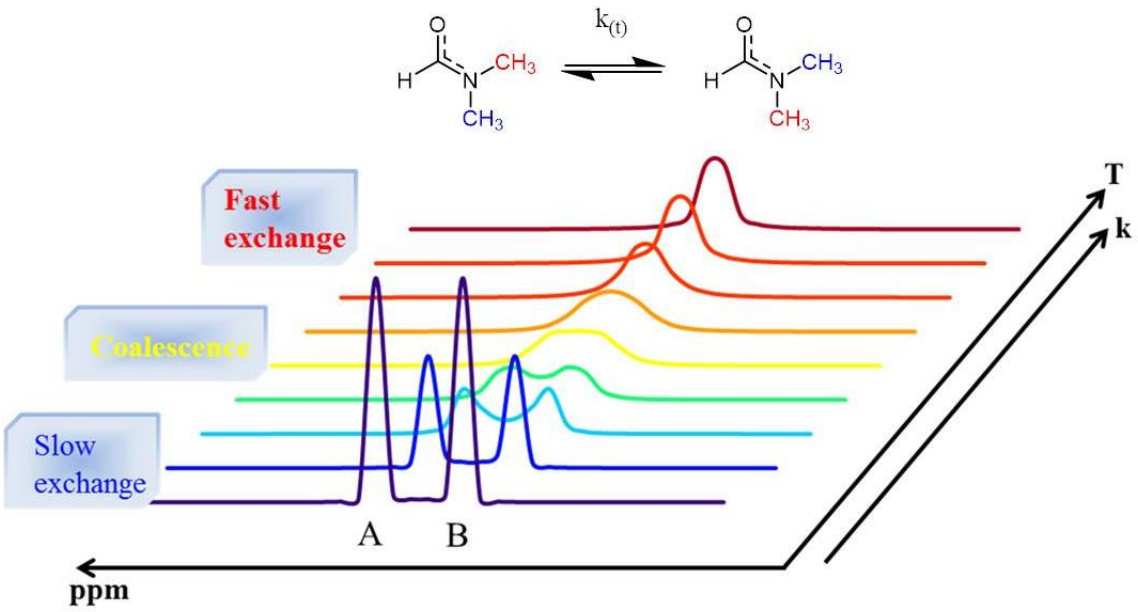

Figure 47: D-NMR example of a dimethyl substitued amide, are highlighted the singlet relating to the two methyl groups [Azmanam – Chemistry lab demonstration – *Chemistry Blog*, 2009]

The NMR spectra recorded at different temperatures provide a qualitative indication of the value of the $\Delta E_{(rot)}$ but it is necessary to extrapolate the kinetic constant from the D-NMR analysis to obtain a measure of the energy.

With the simplest systems, it is possible to use the equation:

$$k_{(Tc)} = \pi \frac{\Delta v}{\sqrt{2}} \qquad 1.3$$

$k_{(Tc)}$ = rate constant at the coalescence temperature (T_c)

This equation derives from a first order kinetic equation and represents two nuclei in absence of any coupling. [44]

For a coupled system, the kinetic constant is derived from *line shape simulation* analysis of the D-NMR spectra. This method allows to handle mathematical models that can simulate second-order spectra and quite complex spin systems, first a simulated spectrum is obtained where the dynamic processes are blocked ($k_{(T)} \approx 0$), then the line shape is simulated at a higher temperature by changing the values of the rate constant. Corrections need to be made to consider the temperature dependence of J couplings, chemical shifts and conformers ratio. The best value of the kinetic constant at each temperature is then found by comparison of the experimental with the computated data.[45]

The free rotational energy can be extracted by means of the derived *Eyring-Polanyi equation* [c]

$$\Delta G^{\ddagger} = 4.574 \bullet 10^{-3} \bullet t \left(log_{10} \frac{T}{k_{(T)}} + 10.318\right) \qquad 1.4$$

T = expressed in Kelvin ; $\Delta G^{\ddagger}$ = expressed in kcal/mol

The line shape simulation is more precise because it provides an overall value of the rotational energy at each analysed temperature. [46]

The D-NMR approach can determine energy values between about 4.5 and about 22 kcal/mol by the line shape simulation, this range is defined by: the NMR time scale, the resolution of the spectrum, the technical range of temperature that the instrument can handle and the deuterated solvent boiling point.

It is possible to study the compounds that belong to Class 1 and partially to Class 2 of LaPlante, the racemization of slow interconverting atropisomers is not accessible with this technique. In these cases, other techniques as D-HPLC or kinetic studies can be applied.

The introduction of chiral stationary phase expand the application of the HPLC to stereodynamic measures, that can be applied to the study of stereo labile compounds.

[c] Derives from : $k = \frac{K\, k_b\, T}{h}\, e^{-\frac{\Delta G^{\ddagger}}{RT}}$; K is the transmission coefficient, k_b is the Boltzmann's constant, h is the Planck's constant, rearranged to obtain the $\Delta G^{\ddagger}$ in kcal/mol.
In this calculation it is possible to define if there are entropic changes, studying the $\Delta G^{\ddagger}$ at different temperatures, which are usually neglectable.

Acquiring chromatograms at different temperatures makes it possible to follow the interconversion of molecules that show a rotational energy barriers up to 25-26 kcal/mol, without needing to have a chirality probe as in the case of D-NMR.

Using a chiral column is possible to separate enantiomers thanks to their different interactions with the stationary phase, this also applies to atropisomers. Raising the temperature, the rotation starts in the column while eluting. The competition between atropisomerisation and resolution generates an elution profile with a plateau between the peaks, that increases in intensity by increasing the temperature. The limit is reached when the racemisation has an higher rate than the separation and it is possible to observe the coalescence of the peaks.

Similar to the D-NMR, in the D-HPLC the kinetic constant is evaluated through line shape simulation of the chromatograms recorded at different temperatures. Although different methods can be applied to reproduce the line shape, one of the most reliable is the stochastic model,[47] where the separation is described through a time dependent function, that can be simulated with an appropriate software.

D-HPLC plays an important role substituting the D-NMR technique when diastereotopic nuclei are missed by the chemical system and when the rotational barrier is higher than 21 kcal/mol (to avoid performing D-NMR at a temperature over + 140 °C). However, thermodynamic limits and the proprieties of the mobile phase prevent the determination of high barriers' energies ($\Delta G^{\ddagger} > 26$ kcal/mol).

To define the rotational barriers of very stable atropisomers, it becomes necessary to analyse the interconversion kinetics by examining concentrations' variation of the single enantiomers over time.

Using a preparative HPLC equipped with a chiral stationary phase, it is possible to obtain analysable quantities of a single pure enantiomer. The sample is subjected to high temperature, taking aliquots at set time intervals and then the concentrations' variations are studied by HPLC analysis [Figure 44].

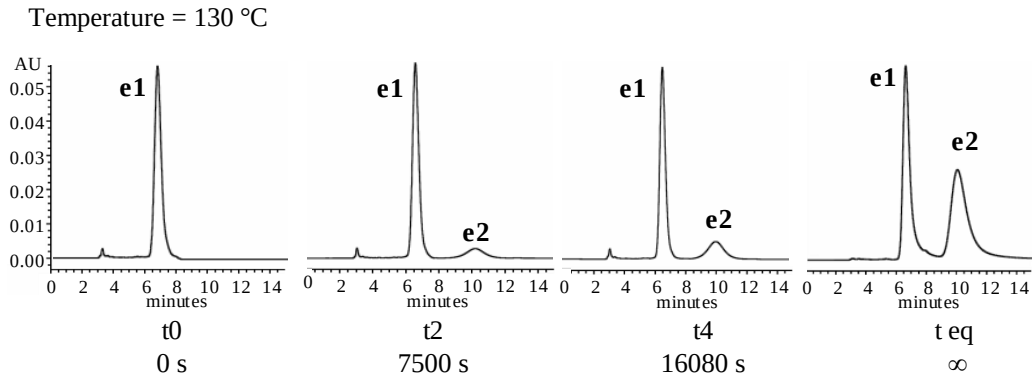

Figure 44: example of concentration variations at time intervals analysed by HPLC

In any racemization process, due to the equal nature of the compounds involved, the rate constant of interconversion of each enantiomers will be the same in both directions. Therefore, the kinetic equation is given considering a first order process at the equilibrium found independent from the initial concentration of the atropisomer.

To define the kinetic constant and therefore the energy barrier:

$$\ln(x_{eq} - x) = -2k_{(T)}\, t + ln\, x_{eq} \qquad 1.1$$

Where x is the molar fraction of **e2** and x_{eq} is the molar fraction of **e2** at the equilibrium (x_{eq} = 0.5).

Plotting $\ln(x_{eq} - x)$ respecting the time (t), the kinetic constant can be obtained through the analysis of the slope, and then it is possible to determine the $\Delta G^{\ddagger}$.

6.3. Analysis of the absolute conformation

Having the possibility to obtain a single enantiomer by HPLC, we use electronic circular dichroism (ECD) compared to quantum mechanical calculations for the analysis of absolute conformation (*P* or *M*). A stable enantiomer is needed to do this type of analysis (Class 3 of LaPlante).

ECD analyses the different capability of chiral molecule to absorb right or left circularly polarized radiation (R-CPL and L-CPL) at wavelength compatible with electronic excitation (UV-Vis, 180 nm to 600 nm). [Figure 45]

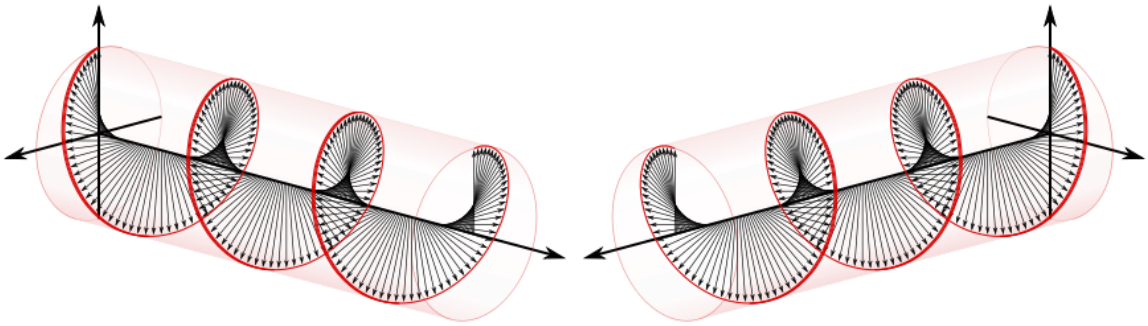

Figure 45: R-CPL and L-CPL, the circularly polarized light condition means a monochromatic electromagnetic radiation where the electronic and the magnetic vector vibrate rotating simultaneously with the propagation direction so as to form a helix. this condition is obtained through instruments called polarimeters [Absorption of Circularly Polarized Light by Supercrystal – ITMO University].

Chiral molecules exhibit circular birefringence, which means that a solution of a chiral substance through which R-CPL and L-CPL are propagated at different speeds. On traversing the circularly birefringent medium, the phase relation between the circularly polarized lights changes and the resultant linearly polarized wave rotates. This is the origin of the phenomenon known as optical rotation.

Circular dichroism (CD) is the difference in the absorption of L-CPL and R-CPL and occurs when a molecule contains one or more chiral chromophores (light-absorbing groups).

The CD signal is composed by the difference: $CD = A^L - A^R$, in other words, the difference between the absorbance of left circular polarized light and right circular polarized light. Usually it is expressed in the difference of molar attenuation coefficient for the L-and R-CPL of the chiral media: $\Delta\varepsilon = \varepsilon^L - \varepsilon^R = \frac{CD}{c\,l}$ because it is independent by the concentration (*c*) and the path length (*l*).

In this regard, the ECD signal reflects the electronic environment of each chromophore and gives important information about the conformation[48]. Moreover, the ECD spectrum is opposite for a pair of enantiomers,[49] which makes this technique to be an ideal candidate for the determination of absolute configuration.

Modern computational techniques can simulate the ECD spectrum for a single enantiomer, comparing the experimental ECD spectrum to a computed one, it is possible to determine the absolute configuration.

To obtain this type of computation, a time dependence density functional theory (TD-DFT) is used. This is an extension of DFT where the conceptual and computational foundations are analogous and it adds the possibility to consider the proprieties of many-body system in the presence of time-dependent potentials, such as electric or magnetic fields.[50]

To perform such calculations, several functionals for TD-DFT were developed. The most common functionals are hybrid ones such as BH&HLYP, M06-2X, ωB97XD which includes empirical dispersion and CAM-B3LYP which includes long range correction using the Coulomb Attenuating Method.[51] To make the best use of these calculations, a very large basis set is required which implies a longer calculation time than the DFT.

A single molecule can populate different conformations as GS without changing its chirality. Since the CD timescale is extremely short, in this case the experimental ECD spectrum is determined by linear combination of ECD spectra of each conformation. To simulate the experimental ECD spectrum properly, all the stable conformations need to be found and their ECD spectra calculated.

Therefore comparing the spectra with the calculations, it is possible to define to each enantiomer its absolute conformation. [Figure 46]

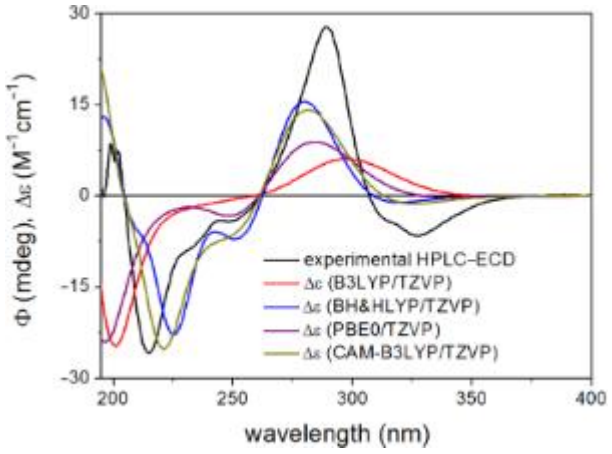

Figure 46: Example of overlapping of the ECD spectra calculated with different functionalities and the one obtained experimentally [Ikei, V.; Spaits, A.; Prechl, A.; Szigetvári, Á.; Béni, Z.; Dékány, M.; Szántay, C., Jr.; Müller, J.; Könczöl, Á.; Szappanos, Á.; Mándi, A.; Antus, S.; Martins, A.; Hunyadi, A.; Balogh, G. T.; Kalaus (†), G.; Bölcskei, H.; Hazai, L.; Kurtán, T. Beilstein *J. Org. Chem*. 2016, vol. 12, 2523–2534]

References

[1] Nancy Argüelles, Eugenia Sánchez-Sandoval, Aarón Mendietad, Lourdes Villa-Tanaca*, Leticia Garduño-Siciliano*, Fabiola Jiménez, María del Carmen Cruz, José L. Medina-Franco*,Germán Chamorro-Cevallos, Joaquín Tamariz* - Design, synthesis, and docking of highly hypolipidemic agents: Schizosaccharomyces pombe as a new model for evaluating a-asarone-based HMG-CoA reductase inhibitors - *Bioorganic & Medicinal Chemistry 18*, **2010,** 4238-4248.

[2] Kenneth R Feingold and Carl Grunfeld - Introduction to lipids and lipoproteins - *Endotext*, **2018**, https://www-ncbi-nlm-nih-gov.ezproxy.unibo.it/books/NBK305896/.

[3] Akira Endo – A historical perspective on the discovery of statins – *The Japan Academy vol. 86*, **2010**, 484-493.

[4] W. David Nes – Biosynthesis of cholesterol and other sterols – *Cem. Rev.*, **2011**, 6423-6451.

[5] The Nobel Prize in Physiology or Medicine 1964. NobelPrize.org. Nobel Media AB 2019. Wed. 23 Jan 2019. <https://www.nobelprize.org/prizes/medicine/1964/summary/> .

[6] The Nobel Prize in Physiology or Medicine 1985. NobelPrize.org. Nobel Media AB 2019. Wed. 23 Jan 2019. https://www.nobelprize.org/prizes/medicine/1985/summary/.

[7] Abc NEWS < https://abcnews.go.com/Health/Wellness/top-selling-statins-equally-effective-study-finds/story?id=14948162 >.

[8] Roitelman J, Olender EH, Bar-Nun S, Dunn WA Jr, Simoni RD. - Immunological evidence for eight spans in the membrane domain of 3-hydroxy-3-methylglutaryl coenzyme A reductase: implications for enzyme degradation in the endoplasmic reticulum.- *J Cell Biol.* **1992**, 959-73.

[9] Jon A Friesen* and Victor W Rodwell - The 3-hydroxy-3-methylglutaryl coenzyme-A (HMG-CoA) reductases - Genome Biology, **2004**, vol. 5 article 248.

[10] Yung-Chi Cheng and William H. Prusoff - Relationship between the inhibition constant (&) and the concentration of inhibitor which causes 50 per cent inhibition (iso) of an enzymatic reaction – *Biochemical Farmacology*, **1973**, vol. 23, 3099-3108

[11] Bruce D. Roth - The Discovery and Development of Atorvastatin, a Potent Novel Hypolipidemic Agent - Prog Med Chem., **2002**; vol. 40 1-22.

[12] Helen M Colhoun, D John Betteridge, Paul N Durrington, Graham A Hitman, H Andrew W Neil, Shona J. Livingstone, Margaret J Thomason, Michael I Mackness, Valentine Charlton-Menys, John H Fuller, on behalf of the CARDS investigators - Primary prevention of cardiovascular disease with atorvastatin in type 2 diabetes in the Collaborative Atorvastatin Diabetes Study (CARDS): multicentre randomised placebo-controlled trial – The Lancet, **2004**, vol. 364: 685–96.

[13] National Health Service - Atorvastatin: a medicine used to lower cholesterol – **2019** https://www.nhs.uk/medicines/atorvastatin/

[14] Jonathan Clayden, Nick Greeves and Stuart Warren – Organic Chemistry – Oxford University Press **2012.**

[15] Oki, M.*Topics in Stereochemistry*, **1983**.

[16] Steven R. LaPlante,* Paul J. Edwards, Lee D. Fader, Araz Jakalian, and Oliver Hucke* - Revealing Atropisomer Axial Chirality in Drug Discovery – *ChemMedChem*, **2011**, vol. 6, 505 – 513

[17] David L. Mobley,* and Ken A. Dill - Binding of Small-Molecule Ligands to Proteins: ‘‘What You See’’ Is Not Always ‘‘What You Get’’ – *Elsevier*, **2009**, 489-498

[18] Garrett M. Morris, Ruth Huey, William Lindstrom, Michel F. Sanner, Richard K. Belew, David S. Goodsell, Arthur J. Olson - AutoDock4 and AutoDockTools4: Automated Docking with Selective Receptor Flexibility - *Journal of Computational Chemistry*, **2009**, 2785-2791

[19] H. Jendralla, E. Baader, W. Bartmann,* G. Beck, A. Bergmann, E. Granzer, B. v. Kerekjarto, K. Kesseler, R. Krause, W. Schubert, and G. Wess - Synthesis and Biological Activity of New HMG-CoA Reductase Inhibitors. 2.Derivatives of 7-(lH-Pyrrol-3-yl)-substituted-3,5-dihydroxy hept-6(E)-enoic (-heptanoic) Acids - *J. Med. Chem.*, **1990**, vol 33 (1), 61–70

[20] Patricia Marce´, James Lynch, A. John Blackerb and Jonathan M. J. Williams* - Conversion of nitroalkanes into carboxylic acids via iodide catalysis in water - *Chem. Commun.*, **2016**, vol. 52, 1013-1016

[21] Yonggui Chi, Li Guo, Nathan A. Kopf, and Samuel H. Gellman – Enantioselective Organocatalytic Michael Addition of Aldehydes to Nitroethylene: Efficient Access to γ2-Amino Acids - *j. Am. Chem. Soc.* **2008**, vol. 130, 5608–5609

[22] Niko S. Radulović, Ana B. Miltojević, Rastko D. Vukićević – simple and efficient one-pot solvent-free synthesis of N-methyl imines of aromatic aldehydes – *C. R Chimie*, **2013**, vol. 16, 257-270
[23] Dale N. Robertson - Phenylnitromethane. I. An Improved Synthesis of a-Nitrostilbenes - *J. Org. Chem.*, **1960**, vol. 25 (1), 47–49
[24] E. A. Ishmaevaa , Ya. A. Vereshchaginaa , D. V. Chachkovb , O. S. Vasil'evac , E. S. Ostroglyadovc , A. A. Nikonorovc , I. A. Litvinovd , D. B. Krivolapovd , A. Z. Alimovaa , and V. M. Berestovitskayac - Polarity and Structure of 2-(1-Methylbenzimidazol-2-yl)- 1-phenyl- and -1,2-Diphenyl-1-nitroethenes – *Russian Journal of General Chemistry*, **2012** , vol. 82 (5), 911-920
[25] E. H. Cordes and W. P. Jencks - On the Mechanism of Schiff Base Formation and Hydrolysis – *J. Am. Chem. Soc.*, **1962**, vol. 84 (5), 832–837
[26] Norman H. Cromwell and Herman Hoeksema - The Synthesis of Some N-Methylbenzylamines and Derivatives - *J. Am. Chem. Soc.*, **1945**, 67 (10), pp 1658–1660
[27] Rajender S. Varma, Rajender Dahiyal and Sudhir Kumar - Microwave-Assisted Henry Reaction: Solventless Synthesis of Conjugated Nitroalkenes – *Tetrahedron Letters*, **1997**, vol. 38, 5131-5134
[28] Jan Otevrel and Pavel Bobal - Diamine-Tethered Bis(thiourea) Organocatalyst for Asymmetric Henry Reaction - *J. Org. Chem.*, **2017**, vol. 82 (16), 8342–8358
[29] Roberto Ballini and Giovanna Bosica - Nitroaldol Reaction in Aqueous Media: An Important Improvement of the Henry Reaction - *J. Org. Chem.*, **1997**, 62 (2), 425–427
[30] Ganesan Bharathiraja, Sekarpandi Sakthivel, Mani Sengoden, and Tharmalingam Punniyamurthy - A Novel Tandem Sequence to Pyrrole Syntheses by 5-endo-dig Cyclization of 1,3-Enynes with Amines - *Org. Lett.*, 2013, vol. 15 (19), 4996–4999
[31] The Nobel Prize in Chemistry 2010. NobelPrize.org. Nobel Media AB 2019. Sat. 16 Feb 2019. <https://www.nobelprize.org/prizes/chemistry/2010/summary/>
[32] Irene Malienda and Oscar Navarro - Recent Developments in the Suzuki-Miyaura Reaction: 2010–2014 – *Molecules*, **2015**, vol. 20(5), 7528-7557
[33] Gary A. Molander,* Paul E. Gormisky, and Deidre L. Sandrock - Scope of Aminomethylations via Suzuki-Miyaura Cross-Coupling of Organotrifluoroborates - *J. Org. Chem.*, **2008**, vol. 73 (6), 2052–2057
[34] Markéta Svobodová , Jan Bárta, Petr Šimunek, Valerio Bertolasi, Vladimír Machácek - Straightforward access to oxazaborines, diazaborinones and triazaborines by reactions of b-enaminoamides with 4-methylbenzenediazonium tetraphenylborate – *J. Organometallic Chem.*, **2009**, vol. 694 (1), 63-71
[35] Mirco Fleige and Frank Glorius – α-Unsubstituted Pyrroles by NHC-Catalyzed Three-Component Coupling: Direct Synthesis of a Versatile Atorvastatin Derivative - *Chem. Eur. J.* **2017**, vol. 23, 10773 – 10776
[36] Norman L. Allinger,* Young H. Yuh, and Jenn-Huei Lii - Molecular Mechanics. The MM3 Force Field for Hydrocarbons - *J. Am. Chem. Soc.*, **1989**,vol. *111* (23), 8551–8566
[37] C. J. Casewit, K. S. Colwell and A. K. Rappé - Application of a Universal Force Field to Main Group Compounds - *J. Am. Chem. Soc.*, **1992**, vol. *114* (25), 10046–10053
[38] Edward M. Engler, Joseph D. Andese, and Paul von R. Schleye - Critical Evaluation of Molecular Mechanics - *J. Am. Chem. Soc.*, **1973**, vol. *95* (24), 8005–8025
[39] Pavarini E., Koch E., Van Den Brink J., Sawatzky G.(eds.) *Quantum Materials: Experiments and Theory Modeling and Simulation Vol. 6* Forschungszentrum Jülich, **2016**
[40] C. C.I. Roothaan – Self-Consistent Field Theory for Open Shells of Electronic System – *Rev. Mod. Phys.*, **1960**, vol. 32, 179-185
[41] L. J. Suam, W. Kohn - One-Particle Properties of an Inhomogeneous Interacting Electron Gas – *Phys. Rev.*, **1966**, vol 145, 561-567
[42] Young, D. Computational Chemistry, chapter 17, pp. 147– 158, Wiley Interscience, New York, **2001**
[43] H. S. Gutowsky, and C. H. Holm - Rate Processes and Nuclear Magnetic Resonance Spectra. II. Hindered Internal Rotation of Amides - *J. Chem. Phys.*, **1956**, vol. 25, 1228-1234
[44] Toyota S., Makino - Rotational isomerism involving an acetylenic carbon. Part 5: Restricted rotation about acetylenic axis in sterically crowded bis(1-phenyl-9-anthryl)ethynes - *T. Tetrahedron Lett.* **2003**, vol. 44, 7775-7778
[45] Brown J. H.; Bushweller C. H., Mastergabin J. C. QCPE Program No. 633, **1993**
[46] Evans, M.G.; Polanyi M. - Some applications of the transition state method to the calculation of reaction velocities, especially in solution - *Trans. Faraday Soc.* **1935**, vol. 31, 875–894
[47] Cirilli R., Costi R., Di Santo R., La Torre F., Pierini M., Siani G. - Perturbing Effects of Chiral Stationary Phase on Enantiomerization Second-Order Rate Constants Determined by Enantioselective Dynamic High-Performance Liquid Chromatography: A Practical Tool to Quantify the Accessible Acid and Basic Catalytic Sites Bonded on Chromatographic Supports - *Anal. Chem.*, **2009**, vol. *81*, 3560-3570

[48] Pescitelli G., Di Bari L., Berova N. - Conformational aspects in the studies of organic compounds by electronic circular dichroism - *Chem. Soc. Rev.* **2011**, vol. *40*, 4603-4625.

[49] Barron L. D., *Molecular Light Scattering and Optical Activity*, Cambridge University Press, Cambridge, 2nd edition **2004**.

[50] Marques, M.A.L.; Gross, E.K.U. – Time-dependent density functional theory - *Annu. Rev. Phys.Chem.* **2004**, vol. *55*, 427-455

[51] Denis Jacquemin, Eric A. Perpe`te, Gustavo E. Scuseria, Ilaria Ciofini, and Carlo Adamo - TD-DFT Performance for the Visible Absorption Spectra of Organic Dyes: Conventional versus Long-Range Hybrids - *J. Chem. Theory Comput.*, **2008**, vol *4* (1), 123–135